Published in final edited form as:
Cell Metab. 2020 August 04; 32(2): 259–272.e10. doi:10.1016/j.cmet.2020.05.019.

Oligodendrocytes Provide Antioxidant Defense Function for Neurons by Secreting Ferritin Heavy Chain

Chaitali Mukherjee[#1,2], **Tina Kling**[#3], **Belisa Russo**[4], **Kerstin Miebach**[5], **Eva Kess**[4], **Martina Schifferer**[2], **Liliana D. Pedro**[1,2], **Ulrich Weikert**[3], **Maryam K. Fard**[2], **Nirmal Kannaiyan**[6], **Moritz Rossner**[6], **Marie-Louise Aicher**[7], **Sandra Goebbels**[7], **Klaus-Armin Nave**[7], **Eva-Maria Krämer-Albers**[5], **Anja Schneider**[4,8,11,*], **Mikael Simons**[1,2,3,9,11,12,*]

[1]Institute of Neuronal Cell Biology, Technical University Munich, 80802 Munich, Germany

[2]German Center for Neurodegenerative Diseases (DZNE), 81377 Munich, Germany

[3]Max Planck Institute of Experimental Medicine, 37075 Göttingen, Germany

[4]German Center for Neurodegenerative Diseases (DZNE), 53127 Bonn, Germany

[5]Institute of Developmental Biology and Neurobiology (IDN), University of Mainz, 55128 Mainz, Germany

[6]Department of Psychiatry, Ludwig-Maximillian University, 80336 Munich, Germany

[7]Department of Neurogenetics, Max Planck Institute of Experimental Medicine, 37075 Göttingen, Germany

[8]Department of Neurodegenerative Diseases and Geriatric Psychiatry, University Bonn, 53127 Bonn, Germany

[9]Munich Cluster of Systems Neurology (SyNergy), 81377 Munich, Germany

[#] These authors contributed equally to this work.

Summary

An evolutionarily conserved function of glia is to provide metabolic and structural support for neurons. To identify molecules generated by glia and with vital functions for neurons, we used

[*]Correspondence: anja.schneider@dzne.de (A.S.), mikael.simons@dzne.de (M.S.).
[11]Senior author
[12]Lead Contact

Author Contributions

M. Simons and A.S. conceived and supervised the project. T.K., C.M., B.R., K.M., E.K., M. Schifferer, L.D.P., U.W., M.K.F., N.K., and M.-L.A. performed experiments and analyzed the data; S.G., K.-A.N., E.-M.K.-A., A.S., and M. Schifferer analyzed the data or supervised data acquisition; and M. Simons wrote the manuscript with input from all authors.

Declaration of Interests

The authors declare no competing interests.

Resource Availabilty

Lead Contact

Further information and requests for resources and reagents should be directed to and will be fulfilled by the Lead Contact, Mikael Simons (mikael.simons@dzne.de).

Materials Availability

All unique reagents generated in this study are available from the Lead Contact with a completed Material Transfer Agreement.

Europe PMC Funders Author Manuscripts

Drosophila melanogaster as a screening tool, and subsequently translated the findings to mice. We found that a cargo receptor operating in the secretory pathway of glia was essential to maintain axonal integrity by regulating iron buffering. Ferritin heavy chain was identified as the critical secretory cargo, required for the protection against iron-mediated ferroptotic axonal damage. In mice, ferritin heavy chain is highly expressed by oligodendrocytes and secreted by employing an unconventional secretion pathway involving extracellular vesicles. Disrupting the release of extracellular vesicles or the expression of ferritin heavy chain in oligodendrocytes causes neuronal loss and oxidative damage in mice. Our data point to a role of oligodendrocytes in providing an antioxidant defense system to support neurons against iron-mediated cytotoxicity.

Introduction

In all complex nervous systems, glia support and modulate neuronal function by executing many vital tasks including the regulation of neurotransmitter metabolism, nutrient supply, and waste disposal (Nave, 2010; Freeman, 2015; Allen and Eroglu, 2017; Liddelow and Barres, 2017; Prinz et al., 2019). For example, long-term axonal survival depends on the supportive function of myelinating oligodendrocytes (Nave and Trapp, 2008; Franklin and Ffrench-Constant, 2008). Several mouse mutants harboring mutations in myelin genes show late-onset axon degeneration in the absence of major myelin alterations, which has raised the question of the underlying mechanisms of such trophic interactions (Griffiths et al., 1998; Lappe-Siefke et al., 2003). One way that oligodendrocytes support axons is by providing lactate and/or pyruvate delivered via monocarboxylate transporter-1 to fuel axonal energy demand (Lee et al., 2012; Fünfschilling et al., 2012). The finding that the metabolic crosstalk between neurons and glia emerged early in evolution, even in unmyelinated species, suggests that trophic interactions are an ancestral function of glia (Shaham, 2006; Freeman, 2015). For example, both in mice and insects glycolytically active glia transfer lactate to neurons to fuel their metabolism (Pellerin and Magistretti, 1994; Lee et al., 2012; Fünfschilling et al., 2012; Volkenhoff et al., 2015). In addition, glia play, across species, a crucial role in establishing and/or maintaining neuronal cell number, axonal ensheathment, neuronal connectivity, and synapse function (Shaham, 2006; Freeman and Rowitch, 2013). In spite of the growing appreciation of neuron-glia interactions as a fundamental aspect of neuronal functions, we lack a full understanding of the actual factors provided by glia with essential function for neurons. Given the high degree of conservation of glial function, we performed RNAi screening in the genetically amenable model organism, *Drosophila melanogaster*, to identify molecules generated by glia with vital functions for neurons. This led to the finding that glia secrete ferritin heavy chain (FTH1), thereby providing an antioxidant defense system to support neurons against iron-mediated cytotoxicity. We extended our study to mice and observed that FTH1 is secreted by oligodendrocytes, which use an unconventional secretion pathway to deliver FTH1 into the extracellular space to protect neurons against oxidative injury. Collectively, our data point to a role of oligodendrocytes in providing an antioxidant defense system to defend neurons against iron-mediated toxicity.

Europe PMC Funders Author Manuscripts

Results

p24-1 in the Secretory Pathway of Glia Is Essential in Maintaining Axonal Integrity

We conducted a genetic screen in *Drosophila melanogaster* to uncover molecules in glia that are essential for axonal integrity. To obtain candidates for the screen, we performed proteome analyses on isolated axogliasomal fractions purified from mice brain on sucrose gradients. From this list, we selected *Drosophila* homologs using the NCBI search tool HomoloGene (https://www.ncbi.nlm.nih.gov/homologene) to identify evolutionarily conserved genes for targeting by glial-specific RNAi. The initial screen included 141 RNAi lines targeting homologous candidate genes (Table S1). We used the UAS/Gal4 system to express RNAi transgenes specifcally in glial cells. Concurrent expression of the reporter CD8-GFP with the panglial driver *re-poGal4* and staining of the neuronal membrane and cytoskeleton allowed us to visualize the fine structure of the peripheral nerves. We performed glia-specific gene silencing and scored for changes of axonal morphology in the third instar larvae nervous system (Figure S1A). Several lines showed axonal defasciculations, but only four developed severe axonal alterations consisting of fragmented and severed axons (Table S2; Figure S1B). To determine glial-specific functions in axonal pathology, we assayed the RNAi lines when crossed to the neuron-specific driver line *n-sybGal4*. We selected *p24-1* as a candidate for further analysis, as only its knockdown in glia, but not in neurons, resulted in severe focal disruptions and axonal swellings along the nerves (Figures 1A and S1C). The p24 protein family, also known as EMP24/GP25L/Erp (endomembrane protein precursor of 24 kD), functions as receptors for shuttling cargo such as GPI-linked proteins or growth factors from the endoplasmic reticulum (ER) to the Golgi apparatus toward the plasma membrane or into the extracellular space (Strating and Martens, 2009). We first confrmed the knockdown effciency of p24-1 by immunohistochemistry (Figure S1D), and then determined the temporal sequence of nerve degeneration (Figure 1B). The pathology started in the frst instar larvae with axonal accumulation of Bruchpilot (Brp)-positive structures, representing vesicles transported from the neuronal cell body in the CNS to the motor synapse (Figures 1D and 1E). Vesicular accumulation was followed by local axonal protrusions with loop-like structures, in which the continuity of the axons was disrupted (Figures 1A and S1E). These results point to a role of p24-1-dependent protein transport in the secretory pathway of glia in maintaining axonal integrity.

Secretion of Ferritin Heavy Chain from Glia Protects against Ferroptosis of Neurons

To determine whether impaired p24-1-dependent cargo transport in glia was responsible for the formation of focal axonal degeneration, we initiated a secondary screen including candidates annotated as “secreted” in the UniProt database or members of the immunoglobulin superfamily (due to their known role in cell interactions and often carrying a GPI anchor). In total, we screened 412 RNAi lines (Table S3), of which only glial knockdown of ferritin 1 heavy chain homolog (*Fer1HCH*) produced a phenotype similar to that observed upon *p24-1* inhibition (Figure 1A). We found focal axonal disruptions and accumulation of Brp-positive vesicles in a temporal sequence as seen after *p24-1* knockdown (Figures 1C, 1F, and 1G). In insects, ferritin is secreted into the extracellular space by transport through the ER and the Golgi apparatus (Nichol et al., 2002). To determine the distribution of Fer1HCH when secreted from glia, we generated a transgenic line expressing

HA-tagged Fer1HCH in glia and found that Fer1HCH-HA was dispersed throughout the peripheral nerve overlapping with the neuronal marker HRP (Pearson's coefficient = 0.44) (Figure S1F). Fer1HCH has ferroxidase activity and functions in iron transport and detoxification (Rouault, 2013). It is possible that glia supply neurons with iron to maintain their energy metabolism. Alternatively, Fer1HCH could play a role in iron detoxifcation. To distinguish between these two possibilities, we treated *repo-Gal4;UAS-Fer1HCH*^{RNAi} and *repo-Gal4:UAS-p24-1*^{RNAi} flies with either the iron salt ferric ammonium citrate (FAC) or the iron chelators deferoxamine (DFO) and bathophenanthrolinedisulfonic acid (BPS). We observed a complete rescue of axonal degeneration by the treatment with both iron chelators, DFO and BPS, but not by FAC, demonstrating that an excess of free iron and not a shortage is responsible for neurodegeneration (Figures 2A–2D). Iron-dependent cell death pathways such as ferroptosis require redoxactive iron for the generation of lipid peroxidation products and lethal reactive oxygen species (ROS) (Dixon et al., 2012). We used lipid peroxidation inhibitors and antioxidants (ferrostatin-1, liproxstatin, and α-tocotrienol) to treat *repo-Gal4;UAS-Fer1HCH*^{RNAi} animals, which resulted in an almost complete rescue of axonal disruptions (Figures 2A–2D). To explore the neuronal response upon RNAi-mediated silencing of *Fer1HCH* in glia, we performed neuron-specific ribosome profiling in transgenic flies expressing the ribosomal protein Rpl10ab under the pan-neuronal driver *n-syb* (Figure S2A). We detected ~9,400 transcripts, of which 1,485 were differentially expressed. KEGG and GO pathway analysis revealed that among the most significantly changed pathways were those involved in metabolism and particularly in oxidoreductase activity, including genes involved in detoxification (Figures S2B and S2C).

Ferritin Heavy Chain Is Secreted from Oligodendrocytes in Association with Extracellular Vesicles

We next tested whether our data in *Drosophila* could be translated into mammalian species, which also express heavy and light chain subunits of ferritin. In the mouse brain, *Fth1*, the subunit containing ferroxidase activity, but not light chain (*Ftl*), transcripts are enriched in oligodendrocytes and found at much lower levels (~20-fold less) in neurons (Todorich et al., 2009; Zhang et al., 2014). *Fth1* transcripts are ranked among the most highly abundant RNAs in oligodendrocytes with the third highest average FPKM values among all transcripts found in these cells (Zhang et al., 2014) and the second highest values detected in purified myelin-enriched membrane fractions (Thakurela et al., 2016). First, we performed immunohistochemistry to determine the expression of FTH1 *in vivo*. We detected FTH1 in the brains of 2- and 6-month-old wild-type mice in a subpopulation of oligodendrocytes (~20%-30% of the CC1-positive oligodendrocytes) (Figures 3A and 3B). At 12 and 24 months of age, a striking increase in FTH1 immunoreactivity was observed, as well as an increase in the fraction of oligodendrocytes that stained positive for FTH1 (~80% of the CC1-positive oligodendrocytes) (Figures 3A and 3B). Next, we performed realtime qPCR on biochemically isolated myelin membrane fractions from wild-type mice and found that *Fth1* transcripts are enriched within myelin fractions as compared to total brain lysates (Figure 3C). Surprisingly, by western blotting we found relatively small amounts of FTH1 protein in myelin compared to brain lysates (Figure 3D). We determined the lifetime of FTH1 in myelin using *in vivo* stable isotope labeling with amino acids (SILAC) (Krüger et al., 2008). Myelin-enriched membrane fractions, obtained from mice that had been fed for 30 and 60

days with the isotopically stable $^{13}C_6$-lysine (SILAC), were subjected to mass spectrometry, followed by mathematical modeling of protein turnover as described (Fard et al., 2017; Fornasiero et al., 2018). While structural myelin proteins such as PLP and MBP are long-lived with lifetimes of ~200 days as expected, the lifetime of FTH1 was only ~17 days (Figure 3E). In addition, compared to PLP and MBP, which have shorter lifetimes in the myelin-depleted membrane fraction, the lifetime of FTH1 did not differ between these two fractions, suggesting that FTH1 does not behave like a myelin-resident protein (Figures 3E and 3F). One possibility to explain the relatively short lifetime and the discrepancy of RNA/protein ratio in myelin is the secretion of FTH1 from oligodendrocytes. In contrast to insects, which release Fer1HCH via the ER to Golgi secretory pathway, mammalian FTH1 lacks a signal peptide and may therefore depend on unconventional secretion pathways such as extracellular vesicle (EV)-dependent release (Truman-Rosentsvit et al., 2018; Mathieu etal., 2019). Using primary cultures of mouse oligodendrocytes, we found that FTH1 co-localized with LAMP-1, a marker for late endosomes and lysosomes, which represent organelles implicated in unconventional secretion pathways (Figure 3G). To determine whether FTH1 was indeed released in association with EVs, we subjected the cell culture medium of primary cultures of oligodendrocytes to sequential centrifugation steps with increasing centrifugal forces to obtain a 100,000*g* pellet, enriched in EVs. Western blotting revealed that FTH1 was readily detected in the 100,000*g* pellet (Figures 3H and 3I). To further validate the secretion of FTH1 in association with EVs, we used oligodendroglial Oli-neu cells, transiently transfected with myc-tagged FTH1. We found that FTH1 was enriched in the EV-enriched fraction prepared from the culture medium, but a fraction of FTH1 was also retained in the supernatant after ultracentrifugation at 100,000*g* (Figure 3J), showing that FTH1 is secreted into two pools, in a non-vesicular fraction and in association with EVs. We determined the amount of free FTH1 secreted by oligodendrocytes into the culture medium, by using an enzyme-linked immunosorbent assay, and estimated that ~3×10^5 oligodendrocytes release ~2 ng of free FTH1 within a few days in culture.

Ferritin Heavy Chain Protects against Ferroptosis

Given that FTH1 is secreted from oligodendrocytes, we next tested whether FTH1 was able to provide neuroprotection by employing previously characterized *in vitro* and *ex vivo* assays of iron-dependent neuronal ferroptosis (Dixon et al., 2012). We used SH-SY5Y neuroblastoma cells and organotypic hippocampal slice cultures, and first confirmed that the iron-chelators, desferrioxamine (DFO) and ciclopirox olamine (CPX), protect against erastin- or L-glutamate-mediated cell death (Figures 4A–4D). We also confirmed that ferrostatin-1 and the noncompetitive N-methyl-D-aspartate (NMDA) receptor antagonist, dizocilpine (MK-801), were protective in erastin- or L-glutamate-induced cell death, respectively. Strikingly, erastin- or L-glutamate-mediated cell death was signifcantly attenuated by the treatment of organotypic hippocampal slice cultures or neuroblastoma cells with recombinant FTH1 (Figures 4A–4D). To determine whether ferroxidase activity of FTH1 was required for the rescue, we generated catalytic inactive FTH1 by substituting two amino acids (E62K and H65G) in the catalytic center (Broxmeyer et al., 1991). We found that mutant recombinant FTH1 devoid of ferroxidase activity failed to provide protection in organotypic hippocampal slice cultures (Figures 4C and 4D). To determine whether physiological amounts of FTH1 could provide protection, we added conditioned medium

from primary cultures of oligodendrocytes to erastin-treated SH-SY5Y neuroblastoma cells. Conditioned medium was able to provide protection, but not when EVs and free FTH1 were depleted from the medium (Figures 4E and 4F).

Oligodendroglial-Derived FTH1 Functions as a Neuroprotective Defense System

As these results pointed to a function of FTH1 in providing neuroprotection, we generated an inducible oligodendrocyte-specific *Fth1* knockout mouse (*Fth1* KO) by crossbreeding PLP-CreERT with *Fth1* $^{fl/fl}$ mice. We induced the conditional deletion of FTH1 in oligodendrocytes by injecting tamoxifen into mice at 2 months and analyzed mice at 6 and 12 months of age (Figure S3A). First, we confirmed the deletion of FTH1 in oligodendrocytes by immunohistochemistry (Figures S3B and S3C). Few oligodendrocytes expressed ferritin light chain in wild-type mice, but this fraction increased slightly in *Fth1* KO, whereas the proportion of cells that stained positive for transferrin remained unchanged in *Fth1* KO compared to controls (Figures S3D–S3G). *Fth1* KO mice were vital and showed no obvious defcits. We determined the ultrastructure of myelinated axons but found no differences in the extent of myelination as assessed by g-ratio analysis and also no differences in oligodendrocyte numbers at 6 and 12 months of age (Figures S3H–S3K). When axon ultrastructure was evaluated in *Fth1* KO mice at 12 months, we detected dark axons with dense axoplasm, in which the cytoskeleton and organelles were difficult to distinguish (Figures 5A and 5B). Dark axonal degeneration is linked to cytoskeletal and, in particular, neurofilament breakdown in myelinated axons without aberrant myelin pathology in various models of brain injury (Marques et al., 2003). We performed immunostainings with antibodies against unphosphorylated neurofilament (SMI32), as neurofilaments in healthy myelinated axons are heavily phosphorylated and not stained by SMI32 antibodies (Sternberger and Sternberger, 1983), and found an increase of SMI32 immunoreactivity in the corpus callosum and cortex of *Fth1* KO mice at 6 and 12 months of age (Figures 5C, 5D, and S4A–S4F). We determined whether axonal pathology was accompanied by neuronal cell loss by quantifying the density of NeuN-positive cells in the motor and primary sensory cortex and the striatum, and found that NeuN-positive cell numbers were unchanged in the striatum and the sensory cortex of *Fth1* KO mice as compared to control at 6 months of age (Figures S4G–S4I). However, at 12 months there was a significant reduction of NeuN-positive cells in *Fth1* KO mice in both the motor and sensory cortex as well as the striatum (Figures 5E, 5F, and S4G–S4J). 8-hydroxylated guanine species such as 8-hydroxy-2’-deoxyguanosine (8OHdG) are repair products of oxidized guanine lesions and have been used as markers for DNA damage linked to oxidative stress (Kasai and Nishimura, 1983). There was an increase in these oxidative DNA modifications in NeuN-positive cortical neurons (Figures 5G, 5H, and S4K–S4P), and higher amounts of autofluorescent material, reminiscent of lipofuscin, an aging pigment generated by oxygen-derived free radicals, were seen in neurons of *Fth1* KO mice compared to control (Figures 5I and 5J). Furthermore, immunohistochemistry revealed an increase in CD68- and IBA1-positive microglia in *Fth1* KO mice compared to control (Figures S4Q–S4S). Together, these results establish a role of oligodendroglial-derived FTH1 as an antioxidant defense system for neurons.

Inhibition of Extracellular Vesicle Release from Oligodendrocytes Results in Neuronal Loss

While these experiments provide evidence of a non-cell-autonomous function of FTH1, they do not show whether the secretion of FTH1 from oligodendrocytes is essential for providing neuroprotection. To address this question experimentally *in vivo*, we had to develop a strategy to block EV secretion specifically in oligodendrocytes in mice. We turned to the small GTPase RAB35 as a candidate molecule, as previous work had provided evidence that it regulates EV release from oligodendroglial cells (Hsu et al., 2010). Consistent with these findings and supporting an EV-dependent release of FTH1, transient overexpression of a dominant-negative RAB35 mutant (RAB35 S22N) reduced the recovery of FTH1 from 100,000*g* pellets prepared by sequential centrifugation from culture medium of Oli-neu cells (Figures 6A and 6B). We also used RNAi directed against *Rab35* to validate these findings, and found that knockdown of *Rab35* leads to a reduction of FTH1 in EV-enriched membrane pellets, providing evidence for RAB35 as a candidate molecule involved in regulating EV-dependent secretion of FTH1 in oligodendrocytes (Figures 6C and 6D). To interfere with EV-dependent FTH1 secretion in oligodendrocytes and to determine whether this pathway is involved in providing neuronal protection *in vivo*, we generated a novel mouse line with floxed allele of the *Rab35* gene, which we crossbred to CNP1-Cre transgenic mice, to obtain conditional knockout of *Rab35* in oligodendrocytes (*Rab35* KO) (Figure S5A). Immunoblot analysis for RAB35 protein levels in cerebellar homogenates of *Rab35* KO mice ($Rab35^{fl/fl}$;$Cnp1^{Cre/wt}$) revealed a decrease of RAB35 protein expression as compared to controls ($Rab35^{wt/wt}$;$Cnp1^{Cre/wt}$) (Figures S5B and S5C). Similar results were obtained for *Rab35* mRNA levels in the cerebellum from 6-month-old mice as measured by reverse-transcriptase quantitative real-time PCR (Figure S5D). To determine whether generation of EV is reduced in *Rab35* KO oligodendrocytes, we purified oligodendrocytes from early postnatal brain of *Rab35* KO and control mice and determined EV release into culture medium using nanoparticle tracking analysis. This analysis revealed a significant reduction in the number of EVs in the culture medium of oligodendrocytes prepared from *Rab35* KO mice compared to controls (Figures 6E and 6F). In addition, using antibodies against a panel of different EV marker proteins, we confirmed by western blotting of EV-enriched membrane pellets, obtained by sequential centrifugation steps, the reduced secretion of EVs from *Rab35* KO oligodendrocytes (Figure S6). Finally, and consistent with EV-dependent FTH1 secretion, we found increased immunoreactivity of FTH1 in CC1-positive oligodendrocytes in brain sections of *Rab35* KO mice (Figures 6G and 6H).

Next, we analyzed *Rab35* KO mice by electron microscopy to first assess the extent of myelination, but did not detect any differences of myelination as determined by g-ratio analyses in the corpus callosum of 6- and 12-month-old *Rab35* KO and control mice (Figures S7A and S7B). In addition, average axon diameter and axon diameter distribution did not differ between *Rab35* KO mice and controls (Figures S7C and S7D). However, similar to findings in *Fth1* KO mice, we detected increased immunoreactivity against unphosphorylated neurofilaments in cortex sections of *Rab35* KO using SMI32 antibodies (Figures 7A and 7B). To test for neuron loss in the motor cortex, we performed immunostainings against the neuronal nuclear antigen NeuN using brain sections from 6- and 12-month-old *Rab35* KO mice and controls (Figure 7C). Strikingly, and as seen in *Fth1*

KO mice, a significant reduction of NeuN-positive neurons was observed in the cerebral motor cortex of *Rab35* KO mice at 12 months of age (Figure 7D). A similar trend was already observed at 6 months of age (Figure 7D). We additionally quantified neuron loss in cortical layers I, II/III-IV, V, and VI. Neuronal loss appeared most pronounced in the cortical layers II/III-IV, in both 6- and 12-month-old mice (Figure S7E). Next, we immunolabeled motor cortex sections of 6- and 12-month-old *Rab35* KO and control mice to examine oxidative DNA damage in neurons (Figure 7E) and detected an increase in 8OHdG DNA oxidation in NeuN-positive cortical neurons of *Rab35* KO mice (Figure 7F). To rule out ectopic recombination of CNP1 -Cre in neurons as an underlying reason of the observed phenotype, we used NEX-Cre to delete *Rab35* in excitatory neurons of the forebrain, but found no differences in the density of NeuN-positive neurons in the motor cortex of 12-month-old KO and control mice (Figure S7F). Collectively, these data point to a role of oligodendroglial-derived EVs as an antioxidant defense system for neurons *in vivo*.

Discussion

The function of oligodendrocytes has for a long time been reduced to its role in synthesizing myelin to enable saltatory nerve conduction. However, during the past decade it has become clear that oligodendrocytes and their myelin sheaths are not purely insulating, but metabolically active and functionally connected to the subjacent axons, providing neuronal support, for example, by shuttling metabolic substrates to fuel its energy requirements (Nave, 2010). In line with this concept, we now provide evidence that oligodendrocytes are also part of a neuronal antioxidant defense system, by secreting FTH1 to support iron detoxification. Neurons are especially vulnerable to oxidative stress because of their high oxygen demand, the abundance of redox-active metals such as iron, and the high levels of oxidizable polyunsaturated fatty acids (Rouault, 2013). The non-cell-autonomous function of FTH1 was surprising, as iron metabolism in oligodendrocytes has so far been associated with the generation of myelin, a process that requires the function of several enzymes that depend on iron as an essential co-factor (Todorich et al., 2009). The need of iron during myelination has been demonstrated in animal studies showing that dietary iron restriction reduces the amount of myelin during gestation and early postnatal periods (Yu et al., 1986; Beard et al., 2003). Moreover, dysregulation of oligodendroglial iron metabolism has been identified as a pathobiological mechanism in Pelizaeus-Merzbacher disease (Nobuta et al., 2019). While these studies have focused on developmental and cell-autonomous roles of iron, they do not address additional non-cell-autonomous functions of iron-binding proteins. In fact, iron accumulates with time in the brain, requiring mechanisms to reduce the free, unbound pool, which can generate free radicals and other strongly oxidizing species capable of reacting with lipids, proteins, and nucleic acids (Rouault, 2013). FTH1 provided by oligodendrocytes and secreted into the extracellular space may be part of such a protective system participating in combating the age-dependent increase in oxidative stress within the brain. While a major function of FTH1 is to store iron in a non-toxic form in the cytosol of mammalian cells, the fact that ferritin subunits contain a signal peptide in insects points to additional extra- and/or inter-cellular functions (Nichol et al., 2002), such as cytoprotective antioxidant defense (Balla et al., 1992). This presumably ancestral function of ferritin heavy chain seems to be prevailing in oligodendrocytes. We fnd that oligodendrocytes release

FTH1 into two extracellular pools: in a non-vesicular fraction and in association with EVs. Currently, we do not know whether FTH1 is enclosed within or associates with the surface of EVs. Recently, a secretory pathway was described for double-stranded DNA (dsDNA) and histones involving engulfment by autophagosome followed by merging with multivesicular endosomes, which subsequently fuse with the plasma membrane to release its content in association with EVs and in a non-vesicular fraction (Jeppesen et al., 2019). Cargo such as FTH1 might piggyback on the EV shuttle to facilitate and direct the transport within the extracellular space. The location from which the secretion of EVs and FTH1 occurs is unknown. Previously, the interaction of the axon with myelin has been regarded as a quiescent interface, but it is now clear that active and activity-dependent communication occurs along the length of the internodal axon and the adjacent paranodes (Micu et al., 2018). This arrangement, also referred to as the “axo-myelinic-synapse” (Micu et al., 2018), could support the release of EVs and FTH1. We also do not know where FTH1 acts to protect neurons, but as membrane-impermeable iron chelators are known to efficiently block against iron-mediated cell death (Dixon et al., 2012), it is possible that FTH1 within the extracellular space is sufficient to provide protection. Alternatively, FTH1 may require EVs as carriers for transport to neurons, where they may accumulate in lysosomes or even within the cells to protect their iron-rich environment against harmful reactions. Indeed, transport of oligodendroglial-derived EVs to neurons has previously been shown in cell culture to be neuroprotective (Frühbeis et al., 2013). Oxidative damage initiated by ROS is a major contributor to cytotoxicity that is characteristic to aging (Rouault, 2013). Iron levels increase naturally in the brain during aging, which could contribute to the age-dependent rise of cell death pathways such as ferroptosis (Stockwell et al., 2017). FTH1 associated with EVs may provide a system to protect against such oxidative stress and cytotoxicity, but yet to be identified additional EV cargos are likely to contribute. While oligodendrocytes appear to be one important source of FTH1-mediated iron buffering in the healthy and aging nervous system, ferritin subunits are known to be upregulated in activated microglia in diseases (Keren-Shaul et al., 2017). Whether ferritin is secreted from microglia is not known, but the role of the innate immune system in iron withdrawal and sequestration points rather to a depot function for iron storage within the cell. Nonetheless, release and transfer of fluorescently labeled ferritin from macrophages to other cells have been demonstrated, supporting the concept of intercellular transfer of ferritin in the brain (Schonberg et al., 2012). As iron accumulation has been associated with a large number of neurological disorders, including the most prevalent neurodegenerative and neuroinflammatory diseases, it will be interesting to address in future studies whether oligodendrocytes participate in protecting against iron-mediated cell death pathways such as ferroptosis in these brain disorders (Rouault, 2013; Ward et al., 2014; Stockwell et al., 2017). It will also be important to consider loss of iron detoxification as a factor contributing to neurodegeneration observed in demyelinating diseases (Lassmann et al., 2012; Stephenson et al., 2014).

Limitations of the Study

The full relevance of our findings in *Drosophila* to neuronal cell death pathways in mammalian models requires further studies. While *Fer1HCH* knockdown in glia leads to acute and severe axonal damage that is rescued by inhibitors against ferroptosis in *Drosophila*, oligodendrocyte-specific *Fth1* KO mice have a more subtle phenotype with

slight neuronal damage that only occurs during aging. Thus, it remains to be established whether these cell death pathways are shared and how ferroptosis contributes to neuronal death in aged mice. Further experiments are also required to understand how FTH1 is released, e.g., encapsulated in EVs or by a secretory autophagy pathway, and how and where FTH1 acts to protect neurons.

Star⋆Methods

Key Resources Table

REAGENT or RESOURCE	SOURCE	IDENTIFIER
Antibodies		
rabbit anti-GFP	Thermo Fisher	Cat# A-11122; RRID: AB_221569
mouse anti-repo	Developmental Studies Hybridoma Bank	DSHB Cat# 8D12; RRID: AB_528448
mouse anti-GFP	Developmental Studies Hybridoma Bank	Cat# DSHB-GFP-12A6; RRID: AB_2617417
mouse anti-Brp	Developmental Studies Hybridoma Bank	DSHB Cat# nc82; RRID: AB_2314866
mouse anti-Futsch	Developmental Studies Hybridoma Bank	DSHB Cat# 22c10; RRID: AB_528403
rabbit anti-p24-1	gift from G. Carnery; Texas A&M University, US	N/A
mouse anti-HA (F-7)	Santa Cruz Biotechnology	Cat# sc-7392; RRID: AB_627809
rabbit anti-HA	Abcam	Cat# ab9110; RRID: AB_307019
mouse anti-Myc	Sigma-Aldrich	Cat# M4439; RRID: AB_439694
rabbit anti-GFP	Thermo-Scientific	Cat# A-6455; RRID: AB_221570
rabbit anti-Calnexin	Enzo	Cat# ADI-SPA-865; RRID: AB_10618434
rabbit anti-FTH1	Abcam	Cat# ab65080; RRID: AB_10564857
rabbit anti-PLP	Laboratory of Klaus-Armin Nave	N/A
mouse anti-ATPaseA1	Abcam	Cat# ab176858; RRID: AB_2802122
mouse anti-CNP	Sigma-Aldrich	Cat# SAB1405637; RRID: AB_10741915
mouse anti-Alix (49/AIP1)	BD Biosciences	Cat# 611620; RRID: AB_399062
mouse anti-TSG101(4A10)	GeneTex	Cat# GTX70255; RRID: AB_373239
rabbit anti-Flotilin	Sigma	Cat# F1180; RRID: AB_1078893
rabbit anti-GAPDH	Thermo Fisher Scientific	Cat# A300-639A-T; RRID: AB_2779357
mouse anti-CD81(mouse-B11)	Santa Cruz	Cat# sc-166029; RRID: AB_2275892

Europe PMC Funders Author Manuscripts

REAGENT or RESOURCE	SOURCE	IDENTIFIER
rabbit anti-Rab35	Proteintech	Cat# 11329-2-AP; RRID: AB_2238179
mouse anti-MBP	Biolegend	Cat# 836504; RRID: AB_2616694
rat anti-LAMP1	Santa Cruz	Cat# sc-19992; RRID: AB_2134495
chicken anti-NeuN	Milipore	Cat# ABN91; RRID: AB_11205760
rabbit anti-NeuN	Abcam	Cat# ab104225; RRID: AB_10711153
mouse anti-CC1	Merck Calbiochem	Cat# OP80; RRID: AB_2057371
rabbit anti-IBA1	WAKO	Cat# 019-19741; RRID: AB_839504
rat anti-CD68 (FA-11)	Biorad	Cat# MCA1957T; RRID: AB_2074849
rabbit anti-7,8-dihydro-8-oxodeoxyguanosine O-H8 (8-OHdG)	Abnova	Cat# MAB6638; RRID: AB_10698211
mouse anti-SMI 32	Merck	Cat# NE1023-100UL; RRID: AB_10682557
rabbit anti-Transferrin	Thermofisher Scientific	Cat# PA3-913; RRID: AB_889484
rabbit anti-Ferritin light chain	Abcam	Cat# ab69090; RRID: AB_1523609
Goat anti-mouse IgG (H+L) secondary antibody, alexa fluor 488,555,647	Thermofisher Scientific	Cat# A-11001; RRID: AB_2534069, A-21422; RRID: AB_2535844, A-21235; RRID: AB_2535804
Alexa Fluor 647-conjugated AffiniPure Donkey Anti-Rat IgG (H+L)	Jackson ImmunoResearch	Cat# 712-605-150; RRID: AB_2340693
Goat anti-rabbit IgG (H+L) secondary antibody, alexa fluor 488,55,647	Thermofisher Scientific	Cat# A-11008; RRID: AB_143165, A-21428; RRID: AB_2535849, A-21244; RRID: AB_2535812
Goat anti-chicken IgY (H+L) Secondary antibody, alexa fluor 647	Thermofisher scientific	Cat# A-21449; RRID: AB_2535866
Anti-mouse/rat/rabbit HRP	Jackson ImmunoResearch	Cat# 115-035-062; RRID: AB_2338504, 112-035-062; RRID: AB_2338133, 111-035-003; RRID: AB_2313567
Chemicals, Peptides, and Recombinant Proteins		
Tamoxifen	Sigma	#T5648
Propidium Iodide - 1.0 mg/mL Solution in Water	ThermeFischerScientific (Invitrogen)	#P3566
Ferrostatin-1	Sigma	#SML0583
Liproxstatin-1	Sigma	#SML1414
a-Tocopherol	Sigma	#T3251
Deferoxamine mesylate salt, powder, 1 g	Sigma	#D9533-1G

REAGENT or RESOURCE	SOURCE	IDENTIFIER
Ferric ammonium citrate	Sigma	#RES20400-A702X
Bathophenanthrolinedisulfonic acid disodium salt hydrate	Sigma	#146617
L-Glutamate Neurotransmitter	Abcam	#ab120049
Erastin, CAS [571203-78-6]	Biozol	#SEL-S7242
Ciclopirox olamine	Sigma	#C2162700
(+)-MK-801 hydrogen maleate	Sigma	#M107
Critical Commercial Assays		
Ovation RNA-Seq System V2	NuGen, Groningen, Netherlands	#7102
IonXpress plus gDNA and Amplicon Library	ThermoFisher	#4471252, #A28950, #4471269, #4474517,
preparation kit		#4476340,and #4482298
Kapa Library Quantification Kit	Roche sequencing solutions	#KK4827
Cell Titer 96 Non-Radioactive Cell Proliferation Assay (MTT)	Promega	# G4100
LIVE/DEAD Viability/Cytotoxicity Kit, for mammalian cells	ThermoFischer Scientifc	#L3224
mouse Ferritin heavy chain (FTH1) ELISA kit	MyBiosource	Cat# MBS931412
Experimental Models: Cell Lines		
Oli-neu cell line	Laboratory of Jacqueline Trotter, IMB Mainz, Germany	RRID: CVCL_IZ82
SH-SY5Y cell line	ATCC	ATCC Cat# CRL-2266; RRID: CVCL_0019
Experimental Models: Organisms/Strains		
Drosophila: w^{1118},	Bloomington Drosophila Stock Center	BSC, #3605; RRID: BDSC_3605
Drosophila: repo-Gal4	Bloomington Drosophila Stock Center	BSC, #7415; RRID: BDSC_7415
Drosophila: n-sybGal4	Bloomington Stock Center	BSC, #51635; RRID: BDSC_51635
Drosophila: n-SybQF.2	Pauli et al., 2008	BSC, #51960; RRID: BDSC_51960
Drosophila: UAS-Ferritin1HCH-HA	This work	N/A
Drosophila: pUAST-Rpl10ab-HA	kindly provided by Herman Dierick, Baylor College of Medicine, US	N/A
Drosophila: nlppGal4	Palm et al., 2012	N/A
Drosophila: UAS-mCD8-GFP	Bloomington Drosophila Stock Center	BSC, #5137; RRID: BDSC_5137
Drosophila: UAS-p24-1^{RNAi}	Vienna Drosophila Resource Center	VDRC, GD#12196
Drosophila: UAS-Fer1HCH^{RNAi}	Vienna Drosophila Resource Center	VDRC, GD#12925
Drosophila: QUAS-HA-Rpl10ab	This work	N/A
Drosophila:;;repoGal4, CD8mCherry, ppkGFP	This work	N/A
Drosophila: ;;repoGal4, n-sybQF.2	This work	N/A

REAGENT or RESOURCE	SOURCE	IDENTIFIER
Drosophila: (on third chromosome)	This work	N/A
RNAi lines used for the genetic screens in this study can be found in Tables S1 and S2	N/A	N/A
Mouse: *B6.129-Fth1$^{tm1.1Lck}$/J*	Jackson's laboratory	RRID: MGI:4848039; Stock No: 018063
Mouse: PLP-CreERT2	U. Sueter, ETH, Zürich, Switzerland	MGI:2663093
Mouse: *Fth1* cKO	This study	N/A
Mouse: *Rab35* cKO ES cells	European Conditional Mouse Mutagenesis	MGI:4436336 Mutant Cell Lines:
(Rab35*m1a(EUCOMM)Hmgu)	Program	HEPD0537_1_G05
Mouse: Flp-deleter (FLIR; Gt(ROSA) 26Sortm1(FLP1)Dym)	Jackson's laboratory	Stock No: 016226; RRID: IMSR_JAX:016226
Mouse: Cnp-Cre (Cnp$^{tm1(cre)Kan}$)	Klaus-Armin Nave, MPI-EM Göttingen, Germany	MGI:3051635
Mouse: NEX-Cre	Klaus-Armin Nave, MPI-EM Göttingen, Germany	Goebbels et al., 2006
Oligonucleotides		
Fth1 genotyping primers, below:		
5'-CCATCAACCGCCAGATCAAC-3'	This paper	N/A
5'-CGCCATACTCCAGGAGGAAC-3'	This paper	N/A
PLP Cre genotyping primers, below:		
5'-TGGACAGCTGGGACAAAGTAAGC-3'	This paper	N/A
5'-CGTTGCATCGACCGGTAATGCAGGC-3'	This paper	N/A
Rab35 genotyping primers, below:		
5'-ACACTTCACATGGCTCTCTGGTCC-3'	This paper	N/A
5'-CTCTAGCAGACCCACAATGCGAGC-3'	This paper	N/A
5'-CAACGGGTTCTTCTGTTAGTCC-3'	This paper	N/A
5'-GCACCATCACCTCTACGTGAGTCC-3'	This paper	N/A
5'-TGAACTGATGGCGAGCTCAGACC-3'	This paper	N/A
CNP Cre genotyping primers, below:		
5'-GCCTTCAAACTGTCCATCTC-3' (CNP-sense)	This paper	N/A
5'-CCCAGCCCTTTTATTACCAC-3' (CNP-antisense)	This paper	N/A
5'-CATAGCCTGAAGAACGAGA-3' (puro3)	This paper	N/A
NEX Cre genotyping primers, below:		
5' -GAGTCCTGGAATCAGTCTTTTTC-3'	This paper	N/A
5'-AGAATGTGGAGTAGGGTGAC-3'	This paper	N/A
5'-CCGCATAACCAGTGAAACAG-3'	This paper	N/A
Fth1 qRT PCR primers		
5'-CAGACCGTGATGACTGGGAG-3'	This paper	N/A
5'-CTCAATGAAGTCACATAAGTGGGG-3'.	This paper	N/A
Atp1a1 qRT PCR primers		
5'-GGCCTTGGAGAACGTGTG-3'	This paper	N/A

REAGENT or RESOURCE	SOURCE	IDENTIFIER
5’-TCGGGAAACTGTTCGTCAG-3’	This paper	N/A
Hrpt qRT PCR primers		
5’-TCCTCCTCAGACCGCTTTT-3’	This paper	N/A
5’-CCTGGTTCATCATCGCTAATC-3’	This paper	N/A
RPLP0 qRT PCR primers		
5’-GATGCCCAGGGAAGACAG-3’	This paper	N/A
5’-ACAATGAAGCATTTTGGATAATCA-3’.	This paper	N/A
Rab35 qRT PCR primers		
5’-TTGCTGTTACGATTCGCAGA-3’	This paper	N/A
5’-AAATCCACTCCGATTGTGGT-3’	This paper	N/A
Recombinant DNA		
pUAST φC31-ready expression vector	kindly provided by Christian Klämbt, University of Münster, Germany	N/A
pQUAST vector	Potter et al., 2010	Addgene #24349
GFP-Rab35 WT	Hsu et al., 2010	N/A
EGFP-Rab35N120I (DN)	Hsu et al., 2010	N/A
FTH1 (Myc-DDK-tagged)-Human ferritin, heavy polypeptide 1 (FTH1)	Origene	CAT#: RC209845
Rab35 siRNA sequences		
ON-TARGETplus non-targeting pool	Dharmacon (Horizon Discovery Group)	#SO-2834792G
UGGUUUACAUGUCGACUAA	N/A	N/A
UGGUUUACAUGUUGUGUGA	N/A	N/A
UGGUUUACAUGUUUUCUGA	N/A	N/A
UGGUUUACAUGUUUUCCUA	N/A	N/A
This ON-TARGETplus SMARTpool (Rab35 targeting)	Dharmacon (Horizon Discovery Group)	#SO-2834792G
UGACGAUGUGUGCCGAAUA	N/A	N/A
ACUAAGUUCCUCACGAUUA	N/A	N/A
AGAAAGACAACUUGGCGAA	N/A	N/A
GUUUAGUGCCGUUAUUUAA	N/A	N/A
Software and Algorithms		
FastQC	Babraham Bioinformatics	https://www.bioinformatics.babraham.ac.uk/projects/fastqc/
Partek Flow	Partek	https://www.partek.com/partek-flow/
DESeq2	Bioconductor	https://bioconductor.org/packages/release/bioc/html/DESeq2.html
Gene Ontologies	GeneOntology	http://geneontology.org/
KEGG PATHWAY Database	KEGG: Kyoto Encyclopedia of Genes and Genomes	https://www.genome.jp/kegg/pathway.html

REAGENT or RESOURCE	SOURCE	IDENTIFIER
imageJ NIH	ImageJ	https://imagej.nih.gov/ij/
GraphPad Prism 7	GraphPad Software	https://www.graphpad.com/
GraphPad Prism (v 5.01)	GraphPad Software	https://www.graphpad.com/
Adobe Illustrator CS5	N/A	https://www.adobe.com/products/illustrator.html
DNASTAR Lasergene 8	N/A	https://www.dnastar.com/software/lasergene/
Bitplane Imaris	N/A	https://imaris.oxinst.com/
Flybase	N/A	http://flybase.org/
Bloomington	N/A	https://bdsc.indiana.edu/
VDRC	N/A	https://stockcenter.vdrc.at/control/main
DPiM	N/A	https://interfly.med.harvard.edu/
Uniprot	N/A	https://www.uniprot.org/
Panther	N/A	httD://pantherdb.org/

Experimental Model and Subject Details

Mice—All experiments performed were in agreement with the German animal welfare law and state specific regulations for animal experiments. The animals were bread and housed in the animal facility of the Max Planck Institute of Experimental Medicine (MPI-EM), Göttingen with 12 h light dark-cycles. The $Fth1^{fl/fl}$ mice were purchased from Jackson's laboratory on C56B6/J background (Darshan et al., 2009). The $Fth1^{fl/fl}$ mice were crossed with mice harboring a tamoxifen inducible Cre-mediated recombination system (Cre-ERT2) driven by PLP promoter (kindly provided by U. Sueter, ETH, Zürich, Switzerland; Leone et al., 2003). Tamoxifen (Sigma T5648) was dissolved in filter-sterilized corn oil to make a solution of 10 mg/mL. The solution was protected from light, and placed on the roller mixer to be dissolved over night at 37°C. It was administrated to the (male only) animals at 2 months of age via intraperitoneal injection once every 24 h for 5 consecutive days as described (Cantuti-Castelvetri et al., 2018). The injection dose was determined by weight, using 75 mg tamoxifen/kg body weight. As control animals we used tamoxifen injected $Fth1^{fl/fl}$; $PLP^{wt/wt}$ mice. The tamoxifen injected $Fth1^{fl/fl}$; $PLP^{wt/wt}$ (control) and $Fth1^{fl/fl}$; $PLP^{CreET2/wt}$ (knockout) mice were further analyzed at 6 months of age (4 months after injection) and at 12 months (10 months after injection). For the targeted disruption of *Rab35* gene, ES cells from a C57BL6 background, harboring a genetically engineered allele of Rab35 with retroviral gene-trap insertion were obtained from European Conditional Mouse Mutagenesis Program (mutant cell line: HEPDO537_1_G05). The targeting vector consisted of a trap cassette with a splice acceptor, a β-galactosidase reporter, a neomycin resistance gene, and a polyadenylation signal. Forconditionally trapped alleles, two pairs of heterotypic recombination sites for the Cre and Flp recombinase were inserted with an inverted orientation on either side of the trap cassette. On chromosome 5, the neomycin resistance gene was flanked by the Frt sites and placed upstream of exon 3 of *Rab35* gene, while exon

3 itself was flanked by loxP sites. The ES cells were further injected into C57BL/6-albino blastocysts. The blastocysts were then implanted in NMRI foster mothers and the resultant chimeric offsprings were identified by coat color and mated to C57BL/6N mice to ensure germline transmission. Following germline transmission and identification of the positive offspring by PCR, the neomycin cassette was deleted by crossing with Flp-deleter mice (= FLIR; Gt(ROSA)26Sortm1(FLP1)Dym), generating mice with the conditional allele Rab35$^{fl/fl}$ mice were crossbred with Cnp-Cre (Lappe-Siefke et al., 2003) or Nex-Cre mice (Goebbels et al., 2006).

For genotyping, animals were subjected to either ear punch or tail biopsies followed by standard DNA extraction methods and PCR amplification protocols with specific primers to identify their correct genotypes. The following primers were used: *Fth1 PCR:* 5'-CCATCAACCGCCAGATCAAC-3' & 5'- CGCCATACTCCAGGAGGAAC-3, *PLP Cre PCR:* 5'-TGGACAGCTGGGACAAAGTAAGC-3 & 5'-CGTTGCATCGACCGGTAATGCAGGC-3. *Rab35 PCR:* 5'-ACACTTCACATGGCTCTCTGGTCC-3', 5'-CTCTAGCAGACCCACA ATGCGAGC-3', 5'-CAACGGGTTCTTCTGTTAGTCC-3', 5'-GCACCATCACCTCTACGTGAGTCC-3' &. 5'-TGAACTGATGGCGAGCT CAGACC-3'. *CNP PCR:* 5'-GCCTTCAAACTGTCCATCTC-3' (CNP-sense), 5'-CCCAGCCCTTTTATTACCAC-3' (CNP-antisense) & 5'-CATAGCCTGAAGAACGAGA-3' (puro3), *Nex Cre PCR:* 5'-GAGTCCTGGAATCAGTCTTTTTC-3', 5'-AGAATGTGGAGTAGGGTG AC-3' &5'-CCGCATAACCAGTGAAACAG-3'. 5'-CCATCAACCGCCAGATCAAC-3' &5'-CGCCATACTCCAGGAGGAAC-3 -3'.

***Drosophila* Stocks—** *Drosophila* stocks were maintained on a standard cornmeal-sugar-agar medium, cornmeal-molasses medium at 18°C and matings performed at 25°C. The following fly stocks were used in combination or recombined in this study: w^{1118}, repo-Gal4 (BSC, #7415) (Sepp and Auld, 1999; Lee and Jones, 2005), n-SybQF.2 (BSC, #51960) (Pauli et al., 2008), lppGal4 (Palm et al., 2012), UAS-mCD8-GFP (BSC, #5137), UAS-p24-1^{RNAi} (VDRC, GD#12196), UAS-Fer1HCH^{RNAi} (VDRC, GD#12925). Other RNAi lines used for the genetic screens in this study can be found in Tables S1 and S2. In total, 503 UAS-dsRNA flies were obtained from Vienna *Drosophila* Resource Centre (VDRC). As a basis for the selection of candidates, a proteome analysis of axogliasomal fractions from mouse brain was performed as described previously (Manrique-Hoyos et al., 2012).

Generation of Transgenic Fly Lines—For the generation of Gal4 effector lines, pUAST ϕC31-ready expression vector was used (kindly provided by Christian Klambt, University of Münster, Germany). cDNA(fer1 hch and p24-1) was amplified from larval mRNA, inserted into pUAST-attB-RfA-3xHA vector and verified by sequencing. The transgenic lines were generated by ϕC31 integrase mediated site-specific recombination system at BestGene. QF.2 effector lines were generated by the following: the attB landing site for C31 germline transformation was cloned in pQUAST (Addgene #24349; Potter et al., 2010) vector over the StuI restriction site. 3xHA-Rpl10ab was amplified from pUAST-HA-Rpl10ab (kindly provided by Herman Dierick, Baylor College of Medicine, US) and cloned over EcoRI-XbaI restriction sites. All transgenes were generated at BestGene using

the phiC31 system (Bischof et al., 2007). Expression of QUAS-3xHA-Rpl10ab construct *in vivo* was confirmed by anti HA-staining of brains of QUAS-HA-Rpl10ab and n-SybQF.2 animals. To allow the simultaneous knockdown of fer1ch in glial cells and overexpression of tagged Rpl10ab in neuronal cells, flies harboring the QUAS-HA-Rpl10ab and the UAS-Fer1HCH-RNAi construct were recombined in one fly line and crossed with the line expressing the two drivers repo-Gal4 and n-syb-QF.2.

Cell Culture

Primary Oligodendrocyte Culture: Primary oligodendrocytes were cultured as previously described (Frühbeis et al., 2013). Briefly, neonatal brain hemispheres from P1 mice pups were stripped free of meninges and trypsinized in 0.25% Trypsin-EDTA solution to single cell suspension. The cells were cultured in Eagle's basal medium with 10% horse serum on poly-L-lysine (PLL) coated flasks at 37°C as a mixed glial culture. After 8-10 days, oligodendrocyte precursors were harvested from the mixed glia cultures using mechanical dissociation. Isolated cells were then cultured in Super-SATO medium (90 mL DMEM with 4.5 g/L glucose, 2 mL 50 × B-27 supplement, 1 mL 200 mM GlutaMAX, 1 mL 100 mM sodium pyruvate, 1 mL heat-inactivated horse serum (HS), 1 mL 5000 U/mL of penicillin/streptomycin, 10 μL 5 mM triiodothyronine, 13 μL 4 mM l-thyroxine) on poly-L-lysine-coated glass coverslips or dishes. Alternatively, oligodendrocytes were prepared by immunopanning as described (Dugas et al., 2010). Briefly, the animals were quickly decapitated and the brains were dissected out and diced into ~1-mm^3 chunks in DPBS without $Ca2^+$/$Mg2^+$ at RT. The brain tissues were dissociated in a papain buffer containing Earle's Balanced Salt Solution (EBSS; Invitrogen) supplemented with 1 mM MgSO4, 0.46% glucose, 2 mM EGTA, 26 mM $NaHCO_3$, 20 units/mL of papain, and 250 units/mL of DNase I. The cell suspension was then transferred for 20 min on a plate coated with rat anti-mouse CD45 (1.25 μg in 12 mL of DPBS/0.2%BSA; BD PharMingen) to deplete remaining microglia. The remaining cell suspension was incubated for 30 min using a rat anti-PDGFRa (rat anti-mouse CD140A, 10 μg in 12 mL of DPBS/0.2% BSA; BD PharMingen) coated plate to isolate oligodendrocytes.

Oli-neu Cell Line: The oligodendroglia precursor cell line (Oli-neu) was cultured as described in Trajkovic et al. (2008). The cells were seeded onto PLL coated Petri dishes and cultured at 37°C with 5% CO_2 in SATO Medium medium supplied with 5% horse serum (DMEM(1x) +− GlutaMAX-1 (highGlucose 4.5g/L D-Glucose), 5% horse serum, 2mM Glutamine, 1mM Sodium Pyruvate, 1x Insuline-Transferrin-Selenium A Supplement, 100 mM Putrescine dihydrochloride, 0.5 mM T3, 0.2 mM Progesterone, 50 U/mL PenStrep). Transient transfections were done using TransIT-LT1 transfection reagent (Mirus) as per the manufacturer's instructions.

SH-SY5Y Cell Line: SH-SY5Y cells were purchased from American type Culture Collection and maintained in DMEM/nutrient mixture F-12 containing 15% fetal bovine serum, 1% non-essential amino acids and 1% penicillin/streptomycin (50,000 cells/mL). All cells were cultured at 37°C in a humidified 5% CO_2 atmosphere.

Organotypic Hippocampal Slice Culture (OHSC): Organotypic hippocampal slices were cultured from P6-8 wildtype C57B6 N mice as previously described (Gerace et al., 2019). 400μm slices were cultured on to Millicell cell culture inserts (0.4 μm pore size; Millipore) placed in 1 mL of culture media (50% Eagle's minimal essential medium, 25% heat-inactivated horse serum, 25% Hanks' balanced salt solution, 5 mg/mL glucose, 2 mM L-glutamine, and 3.75 mg/mL amphotericin B) and cultured according to the interface method (Stoppini et al., 1991). The OHSCs were maintained at 35°C and 5% CO_2 in a humidified incubator. The culture medium was changed every other day.

Method Details

Histology and Image Acquisition—Larvae were dissected as filets preparations to preserve the fine structure of the whole nervous system and fixed for 20 min in 4% paraformaldehyde (PFA) or for 3 min in Bouins's solution (Sigma-Aldrich) followed by standard immuno-labeling procedures. The following antibodies were used: rabbit anti-GFP (1:1000, LifeTechnologies), mouse anti-repo (1D48D12, 1:100), mouse anti-GFP (12A6,1:500), mouse anti-Brp (nc82,1:250), mouse anti-Futsch (22C10,1:250) all from Developmental Studies Hybridoma Bank; rabbit anti-p24-1 (kind gift from G. Carnery; Texas A&M University, US), mouse anti-HA (F7, 1:100, Santa Cruz) and rabbit anti-HA (#9110,1:250, Abcam), and anti-HRP-Alexa637 (1:300, Jackson Immuno Research). Secondary antibodies with Alexa 488, Alexa555 or Alexa647 conjugate (LifeTechnologies) were used in a dilution of 1:1000. Samples were mounted in VectaShield anti fade reagent (H-1000, Vector Laboratories). Confocal images were taken with Zeiss LSM 510 Meta microscope.

RNA Isolation and Sequencing—To evaluate the neuronal response upon Fer1HCH downregulation in glia, we designed a ribosome profiling experiment that allowed the immune-purification of neuronal translating ribosomes by expressing the QUAS-HA-Rpl10ab construct in neuronal cells with n-SybQF.2 driver. The immunoprecipitation of neuronal HA tagged ribosomes of third instar larvae was performed as described (Thomas et al., 2012). Briefly, 3 mL of polysome extraction buffer was prepared freshly by adding 0.5 mM DTT, 100 μg/mL cycloheximide, 1x Complete Protease Inhibitor (Roche) and 100 U/mL RNase OUT (ThermoFisher). Around 200 larval brains were dissected in polysome extraction buffer without RNase OUT and collected in 500 μL of cold polysome extraction buffer. Homogenization was conducted with a pre-cooled pestle and by passing the lysate through needles of increasingly smaller diameter (27 gauge, 23 gauge, 20 gauge). Lysates were incubated for 30 min on ice and finally centrifuged at 100,000 g for 30 min at 4°C. The supernatant was then incubated with the pre-washed magnetic α-HA beads (F-7, Santa Cruz) overnight at 4°C under agitation. Beads were gently washed and resuspended in 400 μL wash buffer. 5 μL 10% RNase-free SDS solution and 5 μL of proteinase K (RNase-free, PeqLab) were added followed by incubation at 55°Cfor 30 min. For RNA extraction, 400 μL Phenol/Chloroform/Isoamylalcohol (acidic, C. Roth) was added and vortexedfor30s(sec). The mixture was transferred to Phase Lock Gel tube (5Prime), mixed by handshaking for 5 min and centrifuged at 14,000 g for 5 min at room temperature (RT). The upper phase was transferred to a fresh Phase Lock Gel tube and the RNA extraction step repeated. The upper phase was transferred to a fresh tube and the RNA was precipitated by adding 0.1 × volumes

of 8M LiCl, 0.007 × volumes of Glycoblue (15 mg/mL) and 3 × volumes of 100% ice cold ethanol. The mix was inverted and incubated for 8-15 h (h) on −20°C. The sample was centrifuged at 16,000 g for 45 min at 4°C. The pellet was washed carefully with 500 μL 70% ethanol and centrifuged 5 min at 4°C. After removal of the ethanol the pellet was dried for 30 to 45 min at 4°C, resuspended in 20 μL RNase-free water and stored at −80°C.

RNA Sequencing and Data Analysis—About 100 ng of isolated RNA was used as input for library generation. cDNA was synthesized using Ovation RNA-Seq System V2 (NuGen, Groningen, Netherlands. Cat No.7102). 100 ng of cDNA was used as input for fragmentation and followed by library preparation using the IonXpress plus gDNA and Amplicon Library preparation kit (ThermoFisher) as described by the manufacturer. The library was then size selected on a 2% E-Gel (ThermoFisher). Sample specific-barcodes were added and amplified subsequently. Individual sample libraries were quantified using Kapa Library Quantification Kit (Kapa, Cat No. KK4827) using 1:200-fold diluted samples. Equal quantities of individual samples were pooled and sequenced on an Ion Proton Sequencer. The reads were split into individual samples based on barcodes and quality controlled using FASTQC tool. The reads were analyzed on Partek Flow software. Briefly, the reads were mapped to *Drosophila melanogaster* genome using TMAP Aligner. The aligned reads were quantified based on dm6 transcriptome annotations. Differential gene expression analysis was performed using DESeq2 Bioconductor R Package. Overrepresentation enrichment analysis and gene set enrichment analysis (GSEA) were performed using KEGG Pathways and Gene Ontologies.

Inhibitor Assay— *Drosophila* larvae were treated with a series of iron-related compounds: ferric ammonium citrate (FAC, 25mM) an iron salt; deferoxamine salt (DFO, 50 μM) and bathophenanthroline disulfonic acid (BPS, 50 μM) iron chelators. Animals were also treated with ferroptosis inhibitors: liprostatin-1 (4 mM), ferrostatin-1 (150 μM) and α-tocotrienol (150 μM). Embryos from the appropriate crossings were collected for 1 h on agar plates containing standard fly food mixed with the corresponding iron-related compounds or ferroptosis inhibitors at 25°C. After hatching, the larvae were counted and selected for the right genotype. Every two days the animals were transferred to fresh plates and food. At the third instar stage, the larvae were dissected and stained with the neuronal marker HRP and the axonal vesicle marker Bruchpilot (Brp).

Myelin Isolation—Myelin from C57BL/6 mouse brains at the ages P20, P75, 6 months and 24 months were purified by sucrose density centrifugation and osmotic shocks as described (Cantuti-Castelvetri et al., 2018). Briefly, the brains were homogenized with an Ultraturrax in 0.32M sucrose including a proteinase inhibitor. The brain lysate in sucrose was added onto 0.85M sucrose and centrifuged with 75,000 g for 30 min. The interphase was washed with diethyl pyrocarbonate (DEPC) water at 75,000 g for 15 min. The pellet was resuspended in water and centrifuged for 15 min at 12,000 g. The washing step, the separation with the sucrose gradient and the second washing were repeated and the pellet was taken up in Quiazol (QIAGEN) and stored at −80°C. Two brains of the 20 days old animals were pooled, the brains of the 75 days old animals were taken individually. The brain lysate was generated from whole brains by homogenization.

Protein Lifetime Measurements—Lifetime measurements were performed as described (Fard et al., 2017; Fornasiero et al., 2018). We used mass spectrometry data obtained from isolated myelin derived from 18 month-old C57BL/6 wildtype mice that had been fed with an isotopically labeled ^{13}C-lysine stable isotope labeling with amino acids (SILAC) diet for 30 or 60 days (Fard et al., 2017). Lifetime measurement was performed as described (Fornasiero et al., 2018). In brief, the ratios of labeled proteins were detected by mass spectrometry and their lifetimes were fitted with a bi-exponential function, with an assumption that the amount of each protein is conserved over time. In order to account for delay in the absorption of the labeled lysines in the living mice, the dynamic changes in the pool of lysines were modeled and taken into consideration during mathematical determination of the lifetimes. All fits are based on the same global parameters of the modeled pool as reported by Fard et al. (2017) and Fornasiero et al. (2018).

RNA Isolation and qRT-PCR—RNA isolation from isolated myelin was performed with the RNeasy mini kit (QIAGEN) according to the manufacturer's instructions and with the following modifications: The myelin was broken up mechanically by mixing it for 10 min on a vortex machine. Isolated RNA was precipitated with Co-precipitant Pink (Bioline). cDNA synthesis was performed with Superscript III reverse transcriptase. The following primers were used:

Fth1-PCR: 5'-CAGACCGTGATGACTGGGAG-3' & 5'-CTCAATGAAGTCACATAAGTGGGG-3'. for normalization: *Atp1a1-PCR:* 5'-GGCCTTGGAGAACGTGTG-3'& 5'-TCGGGAAACTGTTCGTCAG-3', *Hrpt-PCR:* 5'-TCCTCCTCAGACCGCTTTT-3'& 5'-CCT GGTTCATCATCGCTAATC-3', *RPLP0-PCR:* 5'-GATGCCCAGGGAAGACAG-3' & 5'-ACAATGAAGCATTTTGGATAATCA-3'. qRT-PCR was performed with SYBR Green.

For RNA extraction from tissue, 1 mL of Trizol (VWR) per 50-100 mg of tissue was used. Following 5 min incubation at RT, samples were centrifuged at 12,000 g for 10min. Supernatants were mixed with 0.2 mL of chloroform, vortexed and incubated for 2 to 3 min at RT. After centrifugation with 12,000 g at 4°C and for 15min the upper phase was collected in a new tube and 0.5 mL of isopropyl alcohol was added. Following a 10 min incubation at RT, the samples were centrifuged with 12,000 g for 15min at 4°C. The pellet was washed with 1 mL of 75% ethanol, vortexed and centrifuged at 7,500 g for 5 min at 4°C. The resultant pellet was air-dried for 5 to 10min and dissolved in DEPC water with a filter tip. RNA concentration was measured using a NanoDrop system. The Super Script Vilo Master Mix (Invitrogen) was used to generate first-strand cDNA from the extracted RNA according to the manufacturer's instructions. Expression levels of Rab35 in the cerebellum isolated from 6 months old mice were measured by relative reverse transcriptase quantitative real-time PCR (RT-qPCR). The following primers were used: *Rab35* Forward: 5'-TTGCTGTTACGATTCG CAGA-3' and Reverse: 5'-AAATCCACTCCGATTGTGGT-3'. The expression of the target gene (*Rab35*) was measured in relation to internal levels of GAPDH, a housekeeping gene. The quantitative PCR was performed using Power SYBR Green PCR Master Mix (ThermoFisher) according to the manufacturer's instructions. The relative changes in gene expression were analyzed by the ΔCt method and the ratio to the control was calculated.

Transient Transfection and Knockdown of RAB35 in Oli-neu Cells—Oli-neu cells were transiently transfected with indicated plasmids, using TransIT-LT1 transfection reagent (Mirus) according to the manufacturer's instructions. For the delivery of siRNA into Oli-neu cells, Lipofectamine RNAiMAX transfection reagent was used as per manufacterers instructions. For the RAB35 knockdown using RNAi, we used a pool of oligonucleotides that target four different regions of the Rab35 sequence (L-042604-01-0005) and a pool of non-targeting oligoneucleotides (D-001810-10-05) as control (doi: 10.1083/jcb.200911018), from Dharmacon (Horizon Discovery Group).

Extracellular Vesicle Purification and Immunoblotting—Extracellular vesicles (EVs) were harvested from the supernatant of either cultures of primary oligodendrocytes or Oli-neu cells, as previously described (Trajkovic et al., 2008; Frühbeis et al., 2013). EVs were collected under serum-free conditions for 14-24 h. The supernatant media was then collected and centrifuged at 3,000*g* for 10 min followed by two times at 4,000*g* for 10 min. Subsequently it was subjected to centrifugation at 10,000*g* for 30 min and ultracentrifugation at 100,000*g* for 1 h. For immunoblotting the pellets (P100) were resuspended in sample buffer (20% glycerol, 4 mM EDTA, 4% SDS, 4% 2-mercaptoethanol, and 100 mM Tris-HCl, pH 6.8) and boiled at 55-90°C for 5 min. Cell lysates from the cultured cells were prepared by incubating the cells (after supernatant collection) with RIPA buffer supplemented with protease inhibitor cocktail for 10 min on ice. The cells were then scraped, and centrifuged at 10,000*g* for 10 min at 4°C. Equal fractions of the supernatant per condition were mixed with sample buffer before subjecting it to 10 or 12% SDS-PAGE and transfer to nitrocellulose membranes. The membranes were blocked (4% milk in PBS+ 0.1% Tween (PBST), incubated over night with primary antibodies in 3% BSA in PBST and washed with PBST three times. The membranes were subsequently incubated with horseradish peroxidase (HRP)-conjugated secondary antibodies for 30 min at RT. After further washing in PBST, the membranes were imaged using an enhanced chemiluminescence system (Pierce), and bands were quantified using ImageJ software (National Institutes of Health). Primary antibodies used: mouse anti-Myc (Sigma-Aldrich M4439,1:1000), rabbit anti-GFP (Thermo-Scientific A645,1:1000), mouse anti-Calnexin (Enzo ADI-SP4-865, 1:1000) rabbit anti-Calnexin (Millipore AB2301, 1:2000) rabbit anti-FTH1 (Abcam ab65080, 1:1000), rabbit anti-PLP (homemade, 1:10) mouse anti-ATPaseA1 (Abcam, 1:5000), mouse anti-CNP (Sigma-Aldrich, 1:1000), mouse anti-Alix (BD Biosciences, 49/AIP1, 1:1000), mouse anti-TSG101 (Gene-Tex, 4A10, 1:500), rabbit anti-Flotilin (Sigma, F1180, 1:1000), rabbit anti-GAPDH (Biomol, 1:2500), mouse anti-CD81 (Santa Cruz, mouse B11, 1:1000) and rabbit anti-Rab35 (Proteintech 11329-2-AP, 1:500)). Secondary antibodies: anti-mouse-, anti-rabbit-, rat-anti-rat-HRP (Jackson ImmunoResearch, 1:10000). For nanoparticle tracking analysis (NTA), serum-free culture medium was centrifuged at 3,000 g, the supernatant diluted in PBS and analyzed using the Nanosight LM10 system equipped with a green laser (532 nm), asyringe pump and Nanosight 2.3 software (Malvern) at 23°C (temperature control). Measurements were recorded six times for 30 s each. The obtained measurements were analyzed with the NanoSight Tracking Analysis 2.3 software.

Enzyme-Linked Immunosorbent Assay—Supernatants of oligodendrocyte culture media centrifuged at 100,000*g* were subjected to a sandwich ELISA using the mouse Ferritin heavy chain (FTH1) ELISA kit (MyBiosource, Cat# MBS931412) as per the manufacturer's instructions. The kit uses biotin-conjugated antibody specific for FTH1 and avidin conjugated Horseradish Peroxidase for detection. Protein concentration corresponds to the O.D. value measured at 450nm. Known concentrations of the protein (provided in the kit) were used to generate a standard curve to determine the concentration of FTH1 in our samples. Unconditioned medium was used as a reference.

Cell Viability Assay—N-His_6 tagged wild-type mouse FTH1 and catalytic inactive mutant FTH1 (E62K, H65G) were generated by gene synthesis and protein expression was carried out in *E. coli* (BiologicsCorp). Proteins were purified and were > 90% pure as judged by SDS-PAGE analysis and with <0.1 EU/μg endotoxin as determine by gel clot Endotoxin assay. For assessment of cell viability, the SH-SY5Y cells were cultured in 96 well plates and experiments were performed at 70% confluency. Ferroptosis assays were performed with the reagents and protocols as previously described (Zille et al., 2019). 22-26 h following treatment with erastin, or erastin together with either indicated drugs, recombinant protein, primary oligodendrocyte culture media or conditioned media harvested from primary oligodendrocytes, cell viability was determined using the MTT assay kit (Promega), a colorimetric assay to measure cellular metabolic activity. The plates were measured using PowerWave HT Microplate Spectrophotometer (BioTek Instruments). For each biological replicate, 3 technical replicates per condition were measured and averaged. The data points on the graph used for statistics represent the biological replicates. Results obtained from the quantitative cell viability (MTT) were further verified by using the LIVE/DEAD Viability/ Cytotoxicity Assay Kit (Thermo Fisher Scientific) as per the manufacturer's instructions. Images were acquired by fluorescence microscopy at Leica DMi8 fluorescence microscope using the microscope software LAS X. After 10-14 days in culture, OHSCs were subjected to excitotoxic injury as previously described (Dixon et al., 2012) with slight modifications. The slices were treated for 16 h with 1 mM L-glutamate in serum free media (SFM; 75% Eagle's minimal essential medium, 25% Hanks' balanced salt solution, 5 mg/mL glucose, 2 mM L-glutamine, and 3.75 mg/mL amphotericin B). Drugs or protein were added 30 min before L-glutamate treatment. After 16 h the slices were placed in fresh SFM and imaged using Leica SP5 confocal microscopy. Tile scan Z stack images of the entire slice were acquired and the percentage of area occupied by PI staining within each slice was determined using ImageJ NIH. The data points on the graph represent all the slices analyzed per condition, which were pooled from at least three independent slice cultures.

Immunocytochemistry—For immunocytochemistry, oligodendrocytes that were cultured for 5 days *in vitro* (DIV) were fixed with 4% PFA for 15 min at RT, followed by permeabilization with 0.1% Triton X-100 in PBS for 1 min. The fixed cells were further incubated with blocking solution (2.5% fetal calf serum (FCS), 2.5% bovine serum albumin (BSA), 2.5% fish gelatine in phosphate buffer saline (PBS)) for 30 min at RT. Subsequently cells were incubated with primary antibodies diluted in 10% blocking solution for 1 h, followed by washing in PBS and further incubation with secondary antibodies for 1 h at RT. The stained glass coverslips were mounted onto a glass slide with a drop of Mowiol solution

(2.4 g Mowiol, 6 g Glycerol, 6 mL H_2O,12 mL 0.2 M Tris-HCl pH 8.5) and dried overnight in the dark prior to imaging. Primary antibody dilutions used: mouse anti-MBP (Biolegend 836504, 1:1000), rat anti-LAMP1 (Santa Cruz sc-19992, 1:200), rabbit anti-FTH1 (Abcam ab65080, 1:300).

Immunohistochemistry—All animals were anesthetized with an intraperitoneal injection of 14% chloral hydrate followed by transcardial perfusion with 4% paraformaldehyde (PFA) with a MPII mini peristaltic pump (Harvard Apparatus) (flow rate: 3 mL/min). The brains were isolated and post-fxed overnight in 4% PFA and cryoprotected in 30% sucrose in phosphate buffer solution (PBS). The post-fxed tissues were embedded in Tissue-Tek O.C.T., and frozen on dry ice. 30 μm coronal sections were cut using cryostat ThermoFischer Cryostar NX70, collected as free floating sections, and stored in cryoprotection solution at −20°C. For immunolabeling, the free floating sections were washed in PBST (PBS+ 0.2% Tween), followed by permeabilization with PBS+0.5% Triton X-100 for 30 min at RT. The permeabilized sections were blocked in blocking solution (2.5% fetal calf serum (FCS), 2.5% bovine serum albumin (BSA), 2.5% fish gelatin in phosphate buffer saline (PBS)) for 1 h at RT followed by incubation with the primary antibody cocktail in 10% of the same blocking solution, overnight at 4°C. The sections were washed with PBST after the incubation with the primary antibody and subsequently incubated with fluorescent secondary antibodies diluted in 10% of blocking solution for 2 h at RT. All sections were incubated with 4’,6-Diamidino-2-phenylindole (DAPI) at a final concentration of 0.025 μg/mL for 15 min prior to mounting on the slides. The primary antibodies and their working dilutions used in this study are as follows: chicken anti-NeuN (Milipore ABN91,1:500), rabbit anti-NeuN (Abcam ab104225,1:100), rabbit anti-FTH1 (Abcam ab65080, 1:300), mouse anti-CC1 (Merck Cal-biochemOP80,1:500), rabbit anti-IBA1 (WAKO 019-19741,1:500), ratanti-CD68 (Biorad MCA 1957,1:200), rabbit anti-7,8-dihydro-8-oxodeoxyguanosine O-H8 (8-OHdG) (Abnova MAB6638, 1:500), mouse anti-SMI 32 (Merck NW1023, 1:500), rabbit anti-Transferrin (Thermofisher Scientific PA3-913, 1:200) and rabbit anti-Ferritin light chain (Abcam ab69090, 1:200). Secondary antibodies used in the study: Alexa Fluor 488, 555 or 647 conjugated streptavidin secondary antibodies (1:500-1:1000, all Life Technologies).

Electron Microscopy—Brains were fixed by transcardial perfusion with 4% paraformaldehyde (PFA), 2.5% glutaraldehyde in 0.1M phosphate buffer (PB) and 0.5% NaCl and post-fixed in fixative solution overnight. The tissue was then cut into 200-μm-thick vibratome sections and postfixed in a solution of 2% osmium tetroxide, 1.5% potassium ferrocyanide in 0.1 M sodium cacodylate buffer (pH 7.4) for 30 min at RT. Following washing with distilled water the sections were stained with 1% uranyl acetate in water for 1 h, dehydrated in a serial dilution of ethanol, and cleared in acetone, embedded in Epon, and incubated at 60°Cfor24 h. The tissues in Epon blocks were then trimmed and reoriented so that ultrathin (60 nm) cross-sections of the lesion could be cut using the ultramicrotome. Ultrathin sections were collected on formvar-coated copper grids. Transmission Electron Microscopy was performed on a JEM1400+ (JEOL) equipped with a Ruby camera using the software packages TEM Center and ShotMeister.

Europe PMC Funders Author Manuscripts

Quantification and Statistical Analysis

Imaging and Analysis—All images were acquired either with the Leica TCS SP5. The image analysis was done using imageJ NIH software. For each experiment, all the conditions were imaged with identical illumination, laser power and gain parameters. 3-5 non-adjacent region of interest (ROIs) from three non-adjacent brain sections were quantified. All the imaging and quantifications were performed in a blinded manner.

For NeuN density measurements, the tile scans depicting all the layers of the cortex were chosen as ROI. The images were thresholded equally to achieve a binary image. The "Analyze particle" plugin of ImageJ was used to determine NeuN cell numbers within a preselected ROI. Neuron density in *Rab35* KO mice was analyzed by counting the number of $NeuN^+$ cells in a z stack with the "3D object counter" plugin of ImageJ. The particle counts obtained were further normalized to the area of the selected ROI to obtain cell density. For the density measurements of $CC1^+$ cells, images of the corpus callosum from control and knockout mice were equally thresholded and the number of $CC1^+$ particles was measured using the Analyze particles plugin in ImageJ. For the 8-OHdG immunostaining and lipofuscin autofluorescence quantifications the "create selection tool"from ImageJ was used to define the area occupied by NeuN signal as ROI. The same ROI was further used to measure integrated density of 8-OHdG immunostaining or lipofuscin autofluorescence within $NeuN^+$ cells. To calculate the oxidative damage to the DNA in neurons of *Rab35* KO mice, sections were stained with antibodies for 8OHdG and NeuN. Analysis was performed with 8-bit images and the "co-localization" plugin of ImageJ was used. After adjusting the threshold in the different channels the % area of co-localization was obtained. For the SMI32 immunostaining, images were thresholded equally followed by integrated density measurement for SMI32 channel within the ROI, using ImageJ. An in-house designed macro was used for the quantification of fluorescence intensity of FTH1 immunostaining in control versus knockout mice, to quantify the percentage of $IBA1^+$ and $CD68^+$ double-positive cells and measure the percentage of $FTH1^+$ and $CC1^+$ double labeled cells. The macro measures the area occupied and intensities of staining from selected channels of interest within a ROI that has been defined by the user. It also measures the common area occupied by the 2 channels together with intensity measurements of the 2 channels within the common area. All values were always normalized to average of the control condition prior to statistical testing. The values are always represented as fold change compared to control unless indicated otherwise. In order to measure g-ratios and axon calibers, the Grid plug-in from ImageJ was used to randomly select axons. The axonal diameter A (defined by the inner limit of the myelin sheath, as the axon caliber) and the total fiber diameter B (defined by the outer limit of the myelin sheath) were measured. The g-ratio was calculated as g = A/B. For measuring of the diameters the "free handle tool" from ImageJ was used.

Statistics—Statistical analysis was performed using GraphPad Prism 7 (GraphPad Software, Inc.) and GraphPad Prism (v 5.01) software. The number of animals and cultures used for the experiments are as indicated in the bars graphs and figure legends of each figure. The sample distributions were assumed to be normal and no particular statistical tests were used to check for normality within the samples. To compare two groups, a two-tailed Student's t test was employed. One way ANOVA was used and the Tukey's or Dunnett's

post hoc test was performed for multiple comparisons to compare more than two groups, unless as stated otherwise in the figure legends. To compare the interactions between different fly or cell lines or mouse genotypes for more than one parameter, a two way ANOVA followed by Sidak's multiple comparison test was used. A p value of < 0.05 was considered significant in all tests ($p < 0.5$: *, < 0.01: *, < 0.001: *** and < 0.0001: ****). All values are represented as mean ± SD.

Supplementary Material

Refer to Web version on PubMed Central for supplementary material.

Acknowledgments

We are grateful to many colleagues and the *Drosophila* stock centers for sharing fly stocks and plasmids with us. PLPCreERT mice were used in collaboration with Ueli Suter (ETH Zürich, Switzerland). We thank Eugenio Fornasiero for help with lifetime calculations. The work was supported by grants from the German Research Foundation (SCHN1265/1-1, TRR274-1, TRR128-2, SyNergy Excellence Cluster EXC2145, Projekt ID390857198), the ERC (Consolidator Grant to M. Simons, Advanced Grant to K.-A.N.), the BMBF (CMT-net), and the Dr. Miriam and Sheldon G. Adelson Medical Research Foundation.

Data and Code Availability

This study did not generate any code.

References

Allen NJ, Eroglu C. Cell biology of astrocyte-synapse interactions. Neuron. 2017; 96:697–708. [PubMed: 29096081]

Balla G, Jacob HS, Balla J, Rosenberg M, Nath K, Apple F, Eaton JW, Vercellotti GM. Ferritin: a cytoprotective antioxidant strategem of endothelium. J Biol Chem. 1992; 267:18148–18153. [PubMed: 1517245]

Beard JL, Wiesinger JA, Connor JR. Pre- and postweaning iron deficiency alters myelination in Sprague-Dawley rats. Dev Neurosci. 2003; 25:308–315. [PubMed: 14614257]

Bischof J, Maeda RK, Hediger M, Karch F, Basler K. An optimized transgenesis system for Drosophila using germ-line-specific phiC31 integrases. Proc Natl Acad Sci USA. 2007; 104:3312–3317. [PubMed: 17360644]

Broxmeyer HE, Cooper S, Levi S, Arosio P. Mutated recombinant human heavy-chain ferritins and myelosuppression in vitro and in vivo: a link between ferritin ferroxidase activity and biological function. Proc Natl Acad Sci USA. 1991; 88:770–774. [PubMed: 1992468]

Cantuti-Castelvetri L, Fitzner D, Bosch-Queralt M, Weil MT, Su M, Sen P, Ruhwedel T, Mitkovski M, Trendelenburg G, Lütjohann D, et al. Defective cholesterol clearance limits remyelination in the aged central nervous system. Science. 2018; 359:684–688. [PubMed: 29301957]

Darshan D, Vanoaica L, Richman L, Beermann F, Kühn LC. Conditional deletion of ferritin H in mice induces loss of iron storage and liver damage. Hepatology. 2009; 50:852–860. [PubMed: 19492434]

Dixon SJ, Lemberg KM, Lamprecht MR, Skouta R, Zaitsev EM, Gleason CE, Patel DN, Bauer AJ, Cantley AM, Yang WS, et al. Ferroptosis: an iron-dependent form of nonapoptotic cell death. Cell. 2012; 149:1060–1072. [PubMed: 22632970]

Dugas JC, Cuellar TL, Scholze A, Ason B, Ibrahim A, Emery B, Zamanian JL, Foo LC, McManus MT, Barres BA. Dicer1 and miR-219 Are required for normal oligodendrocyte differentiation and myelination. Neuron. 2010; 65:597–611. [PubMed: 20223197]

Fard MK, van der Meer F, Sánchez P, Cantuti-Castelvetri L, Mandad S, Jäkel S, Fornasiero EF, Schmitt S, Ehrlich M, Starost L, et al. BCAS1 expression defines a population of early myelinating oligodendrocytes in multiple sclerosis lesions. Sci Transl Med. 2017; 9

Fornasiero EF, Mandad S, Wildhagen H, Alevra M, Rammner B, Keihani S, Opazo F, Urban I, Ischebeck T, Sakib MS, et al. Precisely measured protein lifetimes in the mouse brain reveal differences across tissues and subcellular fractions. Nat Commun. 2018; 9:4230. [PubMed: 30315172]

Franklin RJ, Ffrench-Constant C. Remyelination in the CNS: from biology to therapy. Nat Rev Neurosci. 2008; 9:839–855. [PubMed: 18931697]

Freeman MR. Drosophila central nervous system glia. Cold Spring Harb Perspect Biol. 2015; 7

Freeman MR, Rowitch DH. Evolving concepts of gliogenesis: a look way back and ahead to the next 25 years. Neuron. 2013; 80:613–623. [PubMed: 24183014]

Frühbeis C, Fröhlich D, Kuo WP, Amphornrat J, Thilemann S, Saab AS, Kirchhoff F, Möbius W, Goebbels S, Nave KA, et al. Neurotransmitter-triggered transfer of exosomes mediates oligodendrocyteneuron communication. PLoS Biol. 2013; 11

Fünfschilling U, Supplie LM, Mahad D, Boretius S, Saab AS, Edgar J, Brinkmann BG, Kassmann CM, Tzvetanova ID, Möbius W, et al. Glycolytic oligodendrocytes maintain myelin and long-term axonal integrity. Nature. 2012; 485:517–521. [PubMed: 22622581]

Gerace E, Landucci E, Bani D, Moroni F, Mannaioni G, Pellegrini-Giampietro DE. Glutamate receptor-mediated neurotoxicity in a model of ethanol dependence and withdrawal in rat organotypic hippocampal slice cultures. Front Neurosci. 2019; 12:1053. [PubMed: 30733663]

Goebbels S, Bormuth I, Bode U, Hermanson O, Schwab MH, Nave KA. Genetic targeting of principal neurons in neocortex and hippocampus of NEX-Cre mice. Genesis. 2006; 44:611–621. [PubMed: 17146780]

Griffiths I, Klugmann M, Anderson T, Yool D, Thomson C, Schwab MH, Schneider A, Zimmermann F, McCulloch M, Nadon N, Nave KA. Axonal swellings and degeneration in mice lacking the major proteolipid of myelin. Science. 1998; 280:1610–1613. [PubMed: 9616125]

Hsu C, Morohashi Y, Yoshimura S, Manrique-Hoyos N, Jung S, Lauterbach MA, Bakhti M, Grønborg M, Möbius W, Rhee J, et al. Regulation of exosome secretion by Rab35 and its GTPase-activating proteins TBC1D10A-C. J Cell Biol. 2010; 189:223–232. [PubMed: 20404108]

Jeppesen DK, Fenix AM, Franklin JL, Higginbotham JN, Zhang Q, Zimmerman LJ, Liebler DC, Ping J, Liu Q, Evans R, et al. Reassessment of exosome composition. Cell. 2019; 177:428–445.e18. [PubMed: 30951670]

Kasai H, Nishimura S. Hydroxylation of the C-8 position of deoxyguanosine by reducing agents in the presence of oxygen. Nucleic Acids Symp Ser. 1983:165–167. [PubMed: 6664853]

Keren-Shaul H, Spinrad A, Weiner A, Matcovitch-Natan O, Dvir-Szternfeld R, Ulland TK, David E, Baruch K, Lara-Astaiso D, Toth B, et al. A unique microglia type associated with restricting development of Alzheimer's disease. Cell. 2017; 169:1276–1290.e17. [PubMed: 28602351]

Krüger M, Moser M, Ussar S, Thievessen I, Luber CA, Forner F, Schmidt S, Zanivan S, Fässler R, Mann M. SILAC mouse for quantitative proteomics uncovers kindlin-3 as an essential factor for red blood cell function. Cell. 2008; 134:353–364. [PubMed: 18662549]

Lappe-Siefke C, Goebbels S, Gravel M, Nicksch E, Lee J, Braun PE, Griffths IR, Nave KA. Disruption of Cnp1 uncouples oligodendroglial functions in axonal support and myelination. Nat Genet. 2003; 33:366–374. [PubMed: 12590258]

Lassmann H, van Horssen J, Mahad D. Progressive multiple sclerosis: pathology and pathogenesis. Nat Rev Neurol. 2012; 8:647–656. [PubMed: 23007702]

Lee BP, Jones BW. Transcriptional regulation of the Drosophila glial gene repo. Mech Dev. 2005; 122:849–862. [PubMed: 15939231]

Lee Y, Morrison BM, Li Y, Lengacher S, Farah MH, Hoffman PN, Liu Y, Tsingalia A, Jin L, Zhang PW, et al. Oligodendroglia metabolically support axons and contribute to neurodegeneration. Nature. 2012; 487:443–448. [PubMed: 22801498]

Leone DP, Genoud S, Atanasoski S, Grausenburger R, Berger P, Metzger D, Macklin WB, Chambon P, Suter U. Tamoxifen-inducible glia-specific Cre mice for somatic mutagenesis in oligodendrocytes and Schwann cells. Mol Cell Neurosci. 2003; 22:430–440. [PubMed: 12727441]

Liddelow SA, Barres BA. Reactive astrocytes: production, function, and therapeutic potential. Immunity. 2017; 46:957–967. [PubMed: 28636962]

Manrique-Hoyos N, Jürgens T, Grønborg M, Kreutzfeldt M, Schedensack M, Kuhlmann T, Schrick C, Brück W, Urlaub H, Simons M, Merkler D. Late motor decline after accomplished remyelination: impact for progressive multiple sclerosis. Ann Neurol. 2012; 71:227–244. [PubMed: 22367995]

Marques SA, Taffarel M, Blanco Martinez AM. Participation of neuroflament proteins in axonal dark degeneration of rat's optic nerves. Brain Res. 2003; 969:1–13. [PubMed: 12676359]

Mathieu M, Martin-Jaular L, Lavieu G, Théry C. Specificities of secretion and uptake of exosomes and other extracellular vesicles for cell-to-cell communication. Nat Cell Biol. 2019; 21:9–17. [PubMed: 30602770]

Micu I, Plemel JR, Caprariello AV, Nave KA, Stys PK. Axo-myelinic neurotransmission: a novel mode of cell signalling in the central nervous system. Nat Rev Neurosci. 2018; 19:49–58. [PubMed: 29118449]

Nave KA. Myelination and support of axonal integrity by glia. Nature. 2010; 468:244–252. [PubMed: 21068833]

Nave KA, Trapp BD. Axon-glial signaling and the glial support of axon function. Annu Rev Neurosci. 2008; 31:535–561. [PubMed: 18558866]

Nichol H, Law JH, Winzerling JJ. Iron metabolism in insects. Annu Rev Entomol. 2002; 47:535–559. [PubMed: 11729084]

Nobuta H, Yang N, Ng YH, Marro SG, Sabeur K, Chavali M, Stockley JH, Killilea DW, Walter PB, Zhao C, et al. Oligodendrocyte death in Pelizaeus-Merzbacher disease is rescued by iron chelation. Cell Stem Cell. 2019; 25:531–541.e6. [PubMed: 31585094]

Palm W, Sampaio JL, Brankatschk M, Carvalho M, Mahmoud A, Shevchenko A, Eaton S. Lipoproteins in Drosophila melanogaster-assembly, function, and influence on tissue lipid composition. PLoS Genet. 2012; 8

Pauli A, Althoff F, Oliveira RA, Heidmann S, Schuldiner O, Lehner CF, Dickson BJ, Nasmyth K. Cell-type-specific TEV protease cleavage reveals cohesin functions in Drosophila neurons. Dev Cell. 2008; 14:239–251. [PubMed: 18267092]

Pellerin L, Magistretti PJ. Glutamate uptake into astrocytes stimulates aerobic glycolysis: a mechanism coupling neuronal activity to glucose utilization. Proc Natl Acad Sci USA. 1994; 91:10625–10629. [PubMed: 7938003]

Potter CJ, Tasic B, Russler EV, Liang L, Luo L. The Q system: a repressible binary system for transgene expression, lineage tracing, and mosaic analysis. Cell. 2010; 141:536–548. [PubMed: 20434990]

Prinz M, Jung S, Priller J. Microglia biology: one century of evolving concepts. Cell. 2019; 179:292–311. [PubMed: 31585077]

Rouault TA. Iron metabolism in the CNS: implications for neurodegenerative diseases. Nat Rev Neurosci. 2013; 14:551–564. [PubMed: 23820773]

Schonberg DL, Goldstein EZ, Sahinkaya FR, Wei P, Popovich PG, McTigue DM. Ferritin stimulates oligodendrocyte genesis in the adult spinal cord and can be transferred from macrophages to NG2 cells in vivo. J Neurosci. 2012; 32:5374–5384. [PubMed: 22514302]

Sepp KJ, Auld VJ. Conversion of lacZ enhancer trap lines to GAL4 lines using targeted transposition in Drosophila melanogaster. Genetics. 1999; 151:1093–1101. [PubMed: 10049925]

Shaham S. Glia-neuron interactions in the nervous system of Caenorhabditis elegans. Curr Opin Neurobiol. 2006; 16:522–528. [PubMed: 16935487]

Stephenson E, Nathoo N, Mahjoub Y, Dunn JF, Yong VW. Iron in multiple sclerosis: roles in neurodegeneration and repair. Nat Rev Neurol. 2014; 10:459–468. [PubMed: 25002107]

Sternberger LA, Sternberger NH. Monoclonal antibodies distinguish phosphorylated and nonphosphorylated forms of neurofilaments in situ. Proc Natl Acad Sci USA. 1983; 80:6126–6130. [PubMed: 6577472]

Stockwell BR, Friedmann Angeli JP, Bayir H, Bush AI, Conrad M, Dixon SJ, Fulda S, Gascón S, Hatzios SK, Kagan VE, et al. Ferroptosis: a regulated cell death nexus linking metabolism, redox biology, and disease. Cell. 2017; 171:273–285. [PubMed: 28985560]

Stoppini L, Buchs PA, Muller D. A simple method for organotypic cultures of nervous tissue. J Neurosci Methods. 1991; 37:173–182. [PubMed: 1715499]

Strating JR, Martens GJ. The p24 family and selective transport processes at the ER-Golgi interface. Biol Cell. 2009; 101:495–509. [PubMed: 19566487]

Thakurela S, Garding A, Jung RB, Müller C, Goebbels S, White R, Werner HB, Tiwari VK. The transcriptome of mouse central nervous system myelin. Sci Rep. 2016; 6

Thomas A, Lee PJ, Dalton JE, Nomie KJ, Stoica L, Costa-Mattioli M, Chang P, Nuzhdin S, Arbeitman MN, Dierick HA. A versatile method for cell-specific profiling of translated mRNAs in Drosophila. PLoS One. 2012; 7

Todorich B, Pasquini JM, Garcia CI, Paez PM, Connor JR. Oligodendrocytes and myelination: the role of iron. Glia. 2009; 57:467–478. [PubMed: 18837051]

Trajkovic K, Hsu C, Chiantia S, Rajendran L, Wenzel D, Wieland F, Schwille P, Brügger B, Simons M. Ceramide triggers budding of exosome vesicles into multivesicular endosomes. Science. 2008; 319:1244–1247. [PubMed: 18309083]

Truman-Rosentsvit M, Berenbaum D, Spektor L, Cohen LA, Belizowsky-Moshe S, Lifshitz L, Ma J, Li W, Kesselman E, Abutbul-Ionita I, et al. Ferritin is secreted via 2 distinct nonclassical vesicular pathways. Blood. 2018; 131:342–352. [PubMed: 29074498]

Volkenhoff A, Weiler A, Letzel M, Stehling M, Klämbt C, Schirmeier S. Glial glycolysis is essential for neuronal survival in Drosophila. Cell Metab. 2015; 22:437–447. [PubMed: 26235423]

Ward RJ, Zucca FA, Duyn JH, Crichton RR, Zecca L. The role of iron in brain ageing and neurodegenerative disorders. Lancet Neurol. 2014; 13:1045–1060. [PubMed: 25231526]

Yu GS, Steinkirchner TM, Rao GA, Larkin EC. Effect of prenatal iron deficiency on myelination in rat pups. Am J Pathol. 1986; 125:620–624. [PubMed: 2432794]

Zhang Y, Chen K, Sloan SA, Bennett ML, Scholze AR, O'Keeffe S, Phatnani HP, Guarnieri P, Caneda C, Ruderisch N, et al. An RNA-sequencing transcriptome and splicing database of glia, neurons, and vascular cells of the cerebral cortex. J Neurosci. 2014; 34

Zille M, Kumar A, Kundu N, Bourassa MW, Wong VSC, Willis D, Karuppagounder SS, Ratan RR. Ferroptosis in neurons and cancer cells is similar but differentially regulated by histone deacetylase inhibitors. eNeuro. 2019; 6

Europe PMC Funders Author Manuscripts

Europe PMC Funders Author Manuscripts

Highlights

- A screen in *Drosophila* identifies glial molecules with vital functions for neurons
- Depletion of glial ferritin heavy chain results in iron-mediated axonal damage
- Ferritin heavy chain is secreted by oligodendrocytes in mice
- Disrupting its release or expression results in neuronal damage in aged mice

Europe PMC Funders Author Manuscripts

Context and Significance

Glia constitute a large fraction of the cells in the central nervous system, but for a long time they were considered merely passive contributors to brain function. This view is changing with the discoveries that glia execute vital tasks in the nervous system, such as providing active support for neuronal survival. Yet the proteins provided by glia and necessary for neuronal viability are incompletely understood. Here, Mukherjee and colleagues identified ferritin heavy chain secreted by glia as an antioxidant defense system supporting neurons against iron-mediated cytotoxicity. Such a system could be important for protecting neurons against oxidative stress in the aging brain or in various neurological diseases.

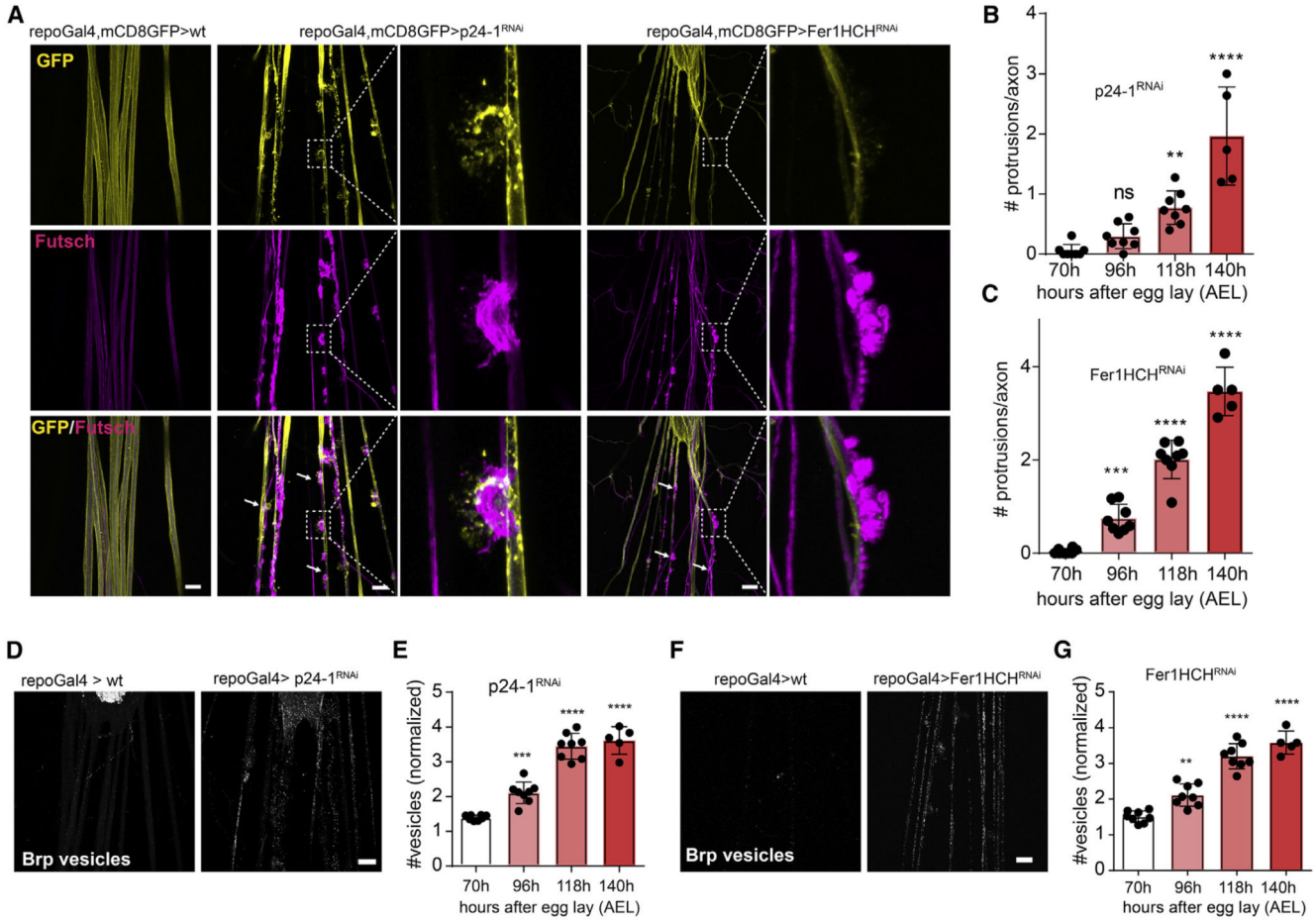

Figure 1. A *Drosophila* Screen Identifies a Function for p24-1 and Ferritin 1 Heavy Chain in Maintaining Axonal Transport and Integrity

(A) Images showing third instar *Drosophila melanogaster* larva peripheral nerves with *repoGal4-driven* CD8-GFP to visualize glia (yellow) and immunostained against the microtubule-associated protein futsch (magenta) to label axons. p24-1 and ferritin 1 heavy chain homolog (*Fer1HCH*) knockdown in glia using *re-poGal4* results in nerve damage with the formation of focal protrusions. White arrows indicate focal axonal degenerations. Insets show higher magnifications of protrusions. Scale bar, 20 μm.

(B and C) Quantification of number of axonal protrusions per nerve afterglial-specific RNAi knockdown of *p24-1* (B) and *Fer1HCH* (C) at second instar(70 h after egg lay [AEL]), mid third instar (96 h AEL), late third instar (118 h AEL), and prolonged third instar larval stages (140 h AEL).

(D) Immunostaining with antibodies against Bruchpilot (Brp) shows the accumulation ofBrp-positivevesicles after glial-specific knockdown of *p24-1* in third instar larvae. Scale bar, 40 μm.

(E) Quantification of Brp-positive vesicles per nerve after glial-specific RNAi knockdown of *p24-1* in second instar (70 h AEL), mid third instar (96 h AEL), late third instar (118 h AEL), and prolonged third instar larval stages (140 h AEL).

(F) Immunostaining with antibodies against Brp shows the accumulation of Brp-positive vesicles after glial-specific knockdown of *Fer1HCH* in third instar larvae as indicated. Scale bar, 20 μm.

(G) Quantification of Brp-positive vesicles per nerve afterglial-specific RNAi knockdown of Fer1HCH in second instar(70 h AEL), mid third instar (96 h AEL), late third instar (118 h AEL), and prolonged third instar larval stages (140 h AEL).

In (E) and (G), the values are normalized to mean of 70 h. All data are means ± SD; ns, non-significant; **p < 0.01, ***p < 0.001, ****p < 0.0001 by one-way ANOVA with Dunnett's multiple comparison test.

See also Figure S1 and Tables S1, S2, and S3.

Europe PMC Funders Author Manuscripts

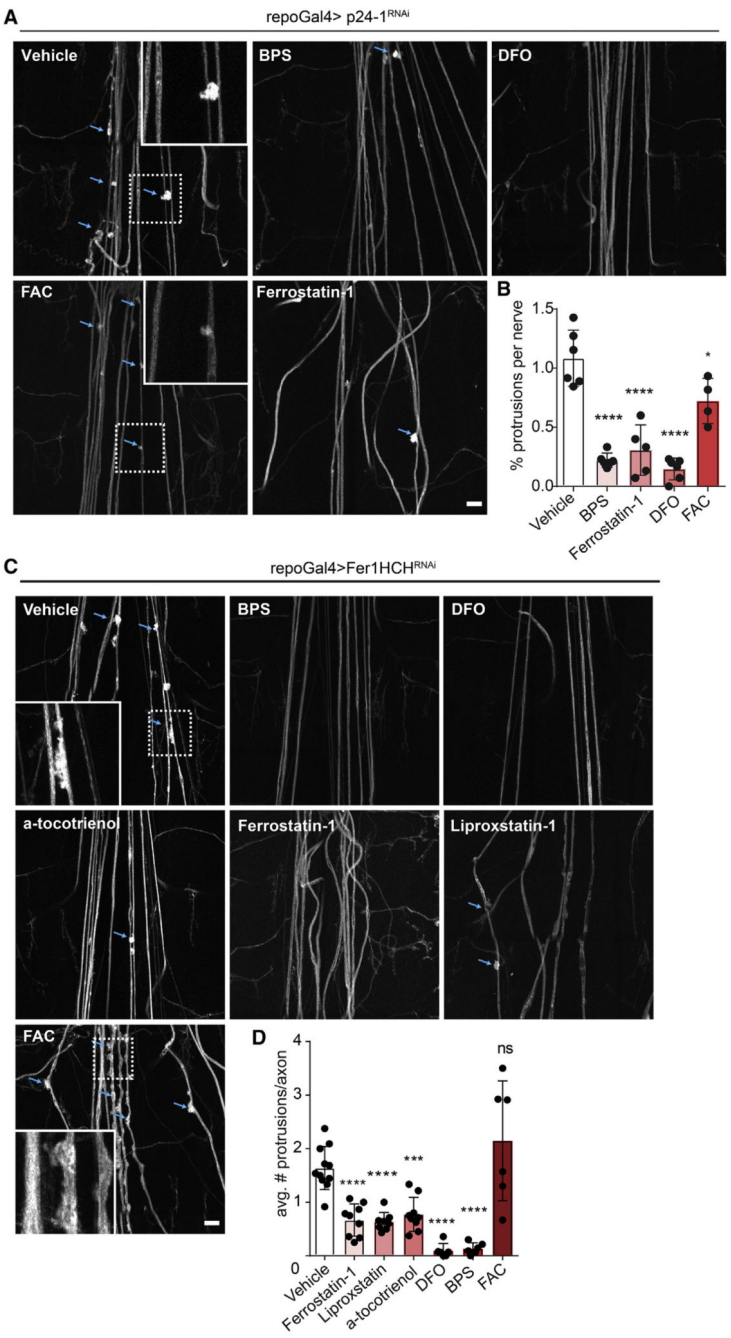

Figure 2. Rescue of p24-1 and Ferritin 1 Heavy Chain Induced Axonal Damage by Iron Chelators and Ferroptosis Inhibitors

(A) Images of the peripheral nervous system of animals treated with vehicle or indicated compounds upon glial-specific p24-1 knockdown. Insets show higher magnifications of protrusions. Scale bar, 40 μm.

(B) Quantification of protrusions per nerve in third instar larva after *p24-1* RNAi knockdown in glia and treatment with vehicle, bathophenanthroline disulfonic acid (BPS; 50 μM), ferrostatin-1 (150 μM), deferoxamine salt (DFO; 50 μM), and ferric ammonium citrate (FAC; 25 mM).

(C) Images of the peripheral nervous system of animals treated with vehicle or indicated compounds upon glial-specific *Fer1HCH* knockdown. Insets show higher magnifcations of protrusions. Scale bar, 40 μm.

(D) Quantifcation of protrusions per nerve in third instar larva after *Fer1HCH* RNAi knockdown in glia and treatment with vehicle, BPS (50 μM), DFO (50 μM), ferrostatin-1 (150 μM), liproxstatin (4 mM), α-tocotrienol (150 μM), and FAC (25 mM).

In (A) and (C), blue arrows indicate axonal protrusions. All data are means ± SD; ns, non-significant; *p < 0.05, ***p < 0.001, ****p < 0.0001 by oneway ANOVA with Dunnett's multiple comparison test.

See also Figure S2.

Europe PMC Funders Author Manuscripts

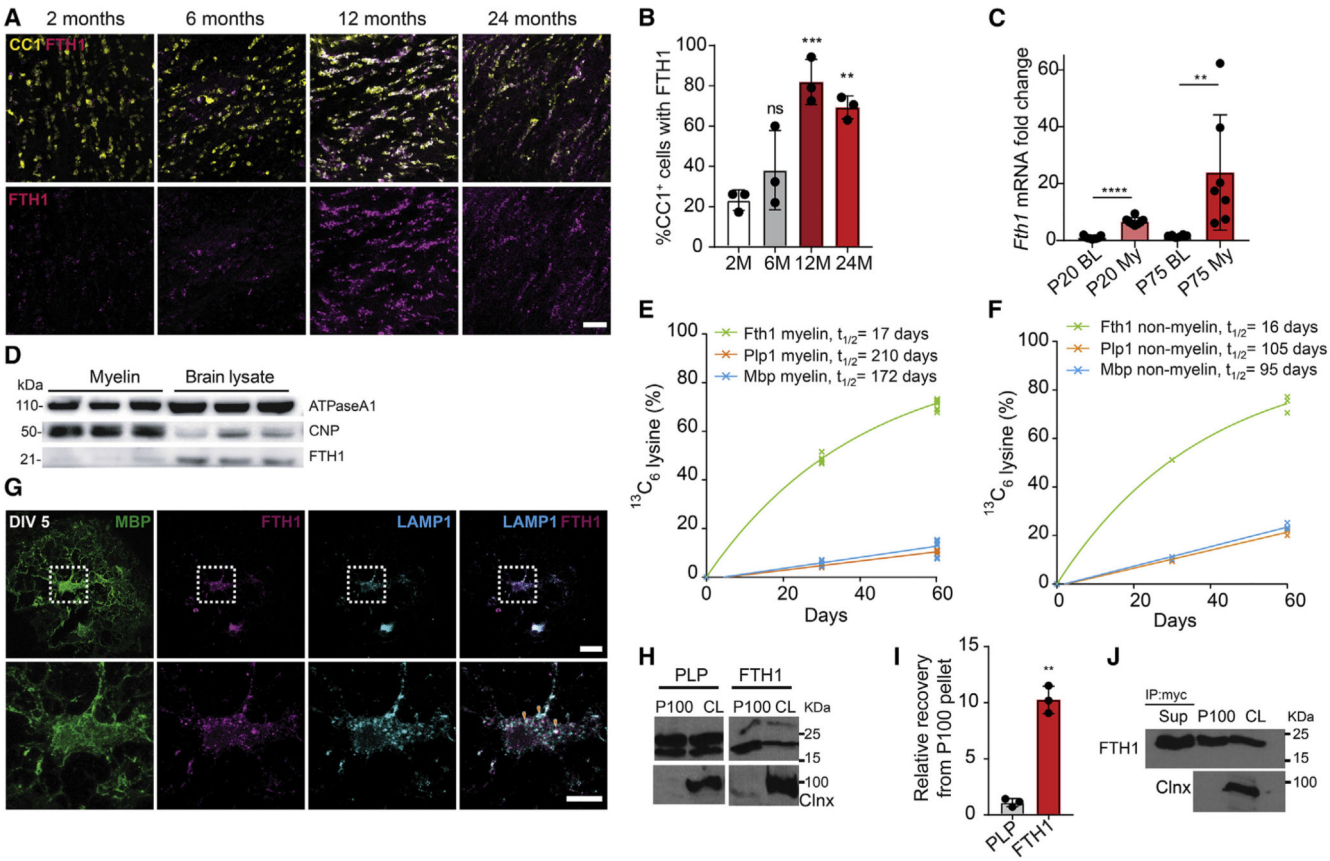

Figure 3. Ferritin Heavy Chain Is Released from Oligodendrocytes and Protects against Neuronal Cell Death

(A) Images of corpus callosum brain sectionsfrom wild-type mice of the indicated ages(2,6,12, and 24 months) immunostained for CC1 (mature oligodendrocyte marker) and FTH1. Scale bar, 50 μm.

(B) Quantification of the percentage of CC1 $^{+}$ cells showing co-labeling with FTH1 at the indicated ages. All data are means ± SD; ns, non-significant; **p < 0.01, ***p < 0.001, by one-way ANOVA with Dunnett's multiple comparison test.

(C) Relative change of *Fth1* mRNA expression in brain lysates (BL) compared to myelin fractions (My) from P20 and P75 wild-type mice. Data are means ± SD; comparison between P20BL versus P20My and P75BL versus P75My by two-tailed unpaired Student's t test. **p < 0.01, ***p % 0.0001.

(D) Immunoblot analyses of brain lysates and myelin fractions obtained from P75 wild-type mice probed with the indicated antibodies.

(E and F) Quantification of protein lifetime for PLP, MBP, and FTH1 in myelin (E) and non-myelin fractions (F).

(G) Representative images of cultured primary oligodendrocytes fixed at 5 days *in vitro* (DIV) and stained for MBP (green), FTH1 (magenta), and LAMP1 (cyan). Lower panel represents higher magnification of indicated (white box) area of the upper panel. Orange arrow heads show FTH1/LAMP1 co-localization. Scale bar, 10 μm.

Europe PMC Funders Author Manuscripts

(H) Western blot of FTH1, PLP, and Calnexin (Clnx) in cell lysates (CL) and the EV-enriched 100,000*g* pellets (P100) of primary cultures of oligodendrocytes. Calnexin was used as a negative control forthe P100 fraction. The membranes were cut at 55 kDa and the respective halves were probed for FTH1 and Calnexin.

(I) Quantification of relative amounts of PLP and FTH1 in P100 normalized to their respective cell lysates. Data are means ± SD; **p < 0.01 by two-tailed paired Student's t test.

(J) Representative western blot of cell lysate (CL), P100, and supernatant of P100 (Sup) fractions immunoprecipited using anti-myc antibody from Oli-neu cells transfected with myc-tagged FTH1. The blot was probed with antibodies against c-*myc* and Calnexin (Clnx).

Europe PMC Funders Author Manuscripts

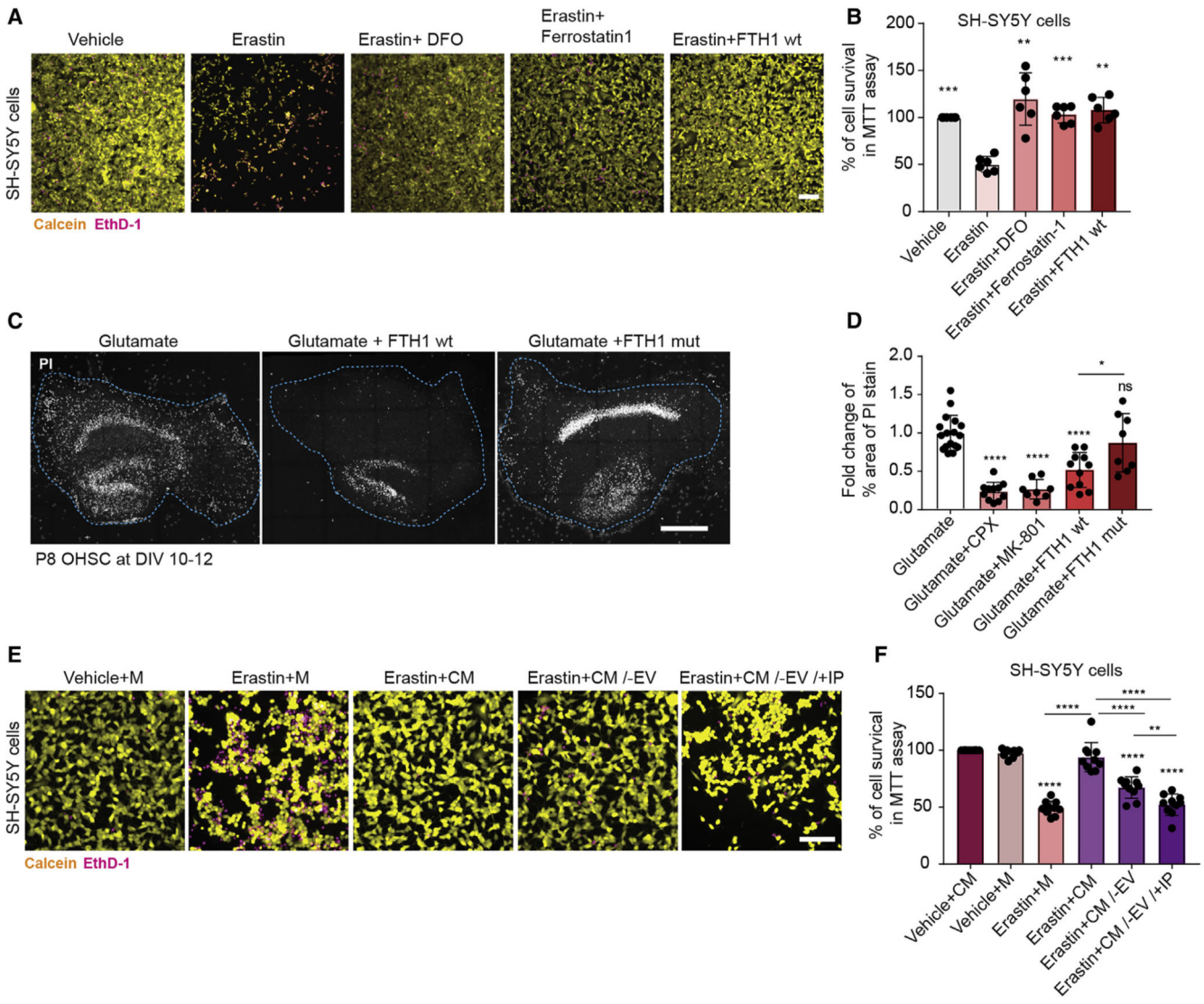

Figure 4. Ferritin Heavy Chain Protects against Ferroptotic Neuronal Cell Death

(A) Images of SH-SY5Y cells treated with vehicle, 20 μM erastin, 20 μM erastin + 50 μM DFO, 20 μM erastin + 10 μM ferrostatin-1, or 20 μM erastin + 10 μg wildtype FTH1. Cells were stained 24 h post treatment with calcein (yellow) to mark living cells and with ethidium homodimer-1 (EthD-1, in magenta) to label dead cells. Scale bar, 100 μm.

(B) Quantification of percentage of living SH-SY5Ycells, following 24 h of treatment with vehicle, 20 μM erastin, 20 μM erastin + 50 μM DFO, 20 μM erastin + 10 μM ferrostatin-1, or 20 μM erastin + 10 μg FTH1wt. The percentage of cell survival was quantified using the colorimetric MTT assay. All data are means ± SD; $^{**}p < 0.01$, $^{***}p < 0.001$ by one-way ANOVA with Dunnett's post hoc test for multiple comparison. All samples were compared to erastin (second column).

(C) Images of organotypic hippocampal slice cultures (OHSC) stained with propidium iodide dye(PI) 16h after being treated with 1 mM glutamate, 40 μgwild-type FTH1 (wt), or catalytically inactive (E62K and H65G) FTH1 mutant (mut). Scale bar, 500 μm.

(D) Quantification of the fold change of percentage of area occupied by dead cells (PI stained cells) after 16 h of treatment as indicated (40 μg FTH1 wt or FTH1 mut, 5 μM ciclopirox olamine [CPX], 10 μM MK-801).

(E) Images ofSH-SY5Y cells treated with vehicle + oligodendrocyte culture media (M), 20 μM erastin + M, 20 μM erastin + oligodendrocyte conditioned medium (CM), 20 μM erastin + 100,000*g* supernatant of CM (CM/−EV), or 20 μM erastin + 100,000*g* supernatant of CM after immunodepletion with FTH1 antibodies to remove free FTH1 (CV/−EV/+IP). Cells were stained 24 h post treatment with calcein (yellow) to mark living cells and with ethidium homodimer-1 (EthD-1, in magenta) to label dead cells. Scale bar, 100 μm.

(F) Quantification of percentage of living SH-SY5Y cells, following 24 h oftreatment with vehicle + CM, vehicle + M, 20 μM erastin + M, 20 μM erastin + CM, 20 μM erastin + CM/−EV, or 20 μM erastin + CM/−EV/+IP. The percentage of cell survival was quantified using the colorimetric MTT assay. All samples were compared to vehicle + CM (first column), unless indicated by lines.

In (D) and (F), all data are means ± SD; ns, non-significant; *$p < 0.05$,**$p < 0.01$,***$p < 0.001$, ****$p < 0.0001$ by one-way ANOVA with Tukey's post hoc test for multiple comparison.

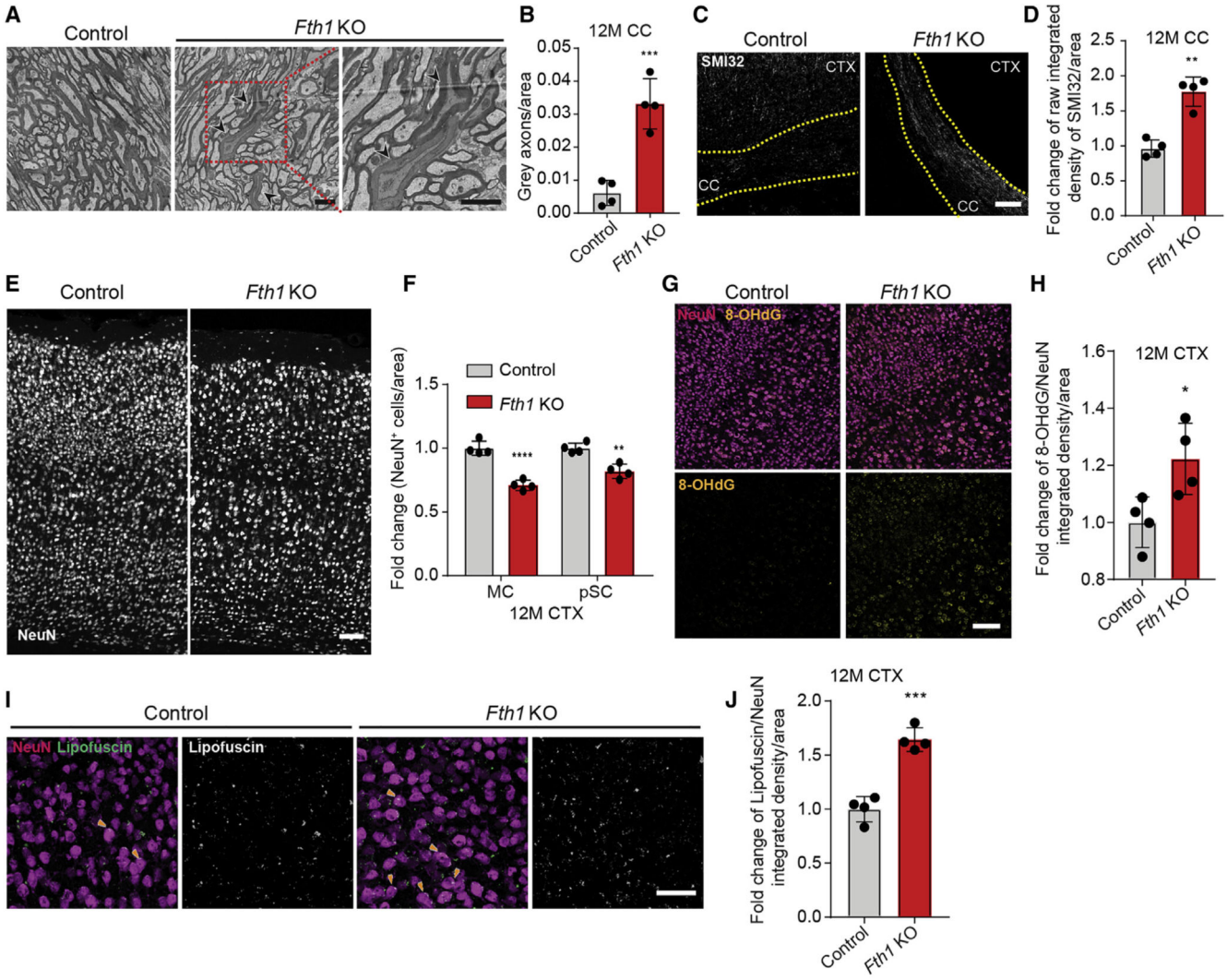

Figure 5. Oligodendrocyte-Specific Ferritin Heavy Chain Knockout Results in Neuronal Loss and Oxidative Damage in Mice

(A) Electron micrograph images of corpus callosum brain sections from 12-month-old oligodendrocyte-specific Fth1 KO ($Fth1^{fl/fl}$;$PLP^{CreERT2/wt}$) and control mice ($Fth1^{fl/fl}$; $PLP^{wt/wt}$) 10 months after tamoxifen induction. Neighboring panel represents higher magnification image of indicated part (red box). Black arrow heads indicate axons with dark cytoplasm. Scale bar, 2 μm.

(B) Quantification of dark axons/area in *Fth1* KO (red) and control (gray) mice at 12 months.

(C) Images of 12-month-old control and *Fth1* KO mice corpus callosum immunostained with antibodies against unphosphorylated neuroflament (SMI32). Scale bar, 100 μm.

(D) Quantifcation of relative SMI32 integrated density per area.

(E) Images of 12-month-old control and *Fth1* KO mice neocortex immunostained with antibodies against neuronal nuclei (NeuN). Scale bar, 100 μm.

Europe PMC Funders Author Manuscripts

(F) Quantification of relative density of $NeuN^+$ cells/area of 12-month-old *Fth1* KO and control mice motor (MC) and primary sensory cortex (pSC). Data are means ± SD; **p < 0.01, ****p < 0.0001 by two-way ANOVA with Sidak's multiple comparison test.
(G) Images of 12-month-old control and *Fth1* KO mice neocortex immunostained with antibodies recognizing oxidative DNA modifications (8-OHdG, yellow) and NeuN (magenta). Scale bar, 100 μm.
(H) Quantification of relative 8-OHdG integrated density per $NeuN^+$ area.
(I) Images of autofluorescent lipofuscin (white) in $NeuN^+$ cells (magenta) in neocortex of 12-month-old *Fth1* KO and control mice. Orange arrow heads indicate lipofuscin (white) accumulated inside $NeuN^+$ cell bodies. Scale bar, 50 μm.
(J) Quantification of relative lipofuscin fluorescence integrated density per $NeuN^+$ area.
In (B), (D), (F), (H), and (J), all data are means ± SD; *p < 0.05, **p < 0.01, ***p < 0.001 by two-tailed Student's t test.
See also Figures S3 and S4.

Europe PMC Funders Author Manuscripts

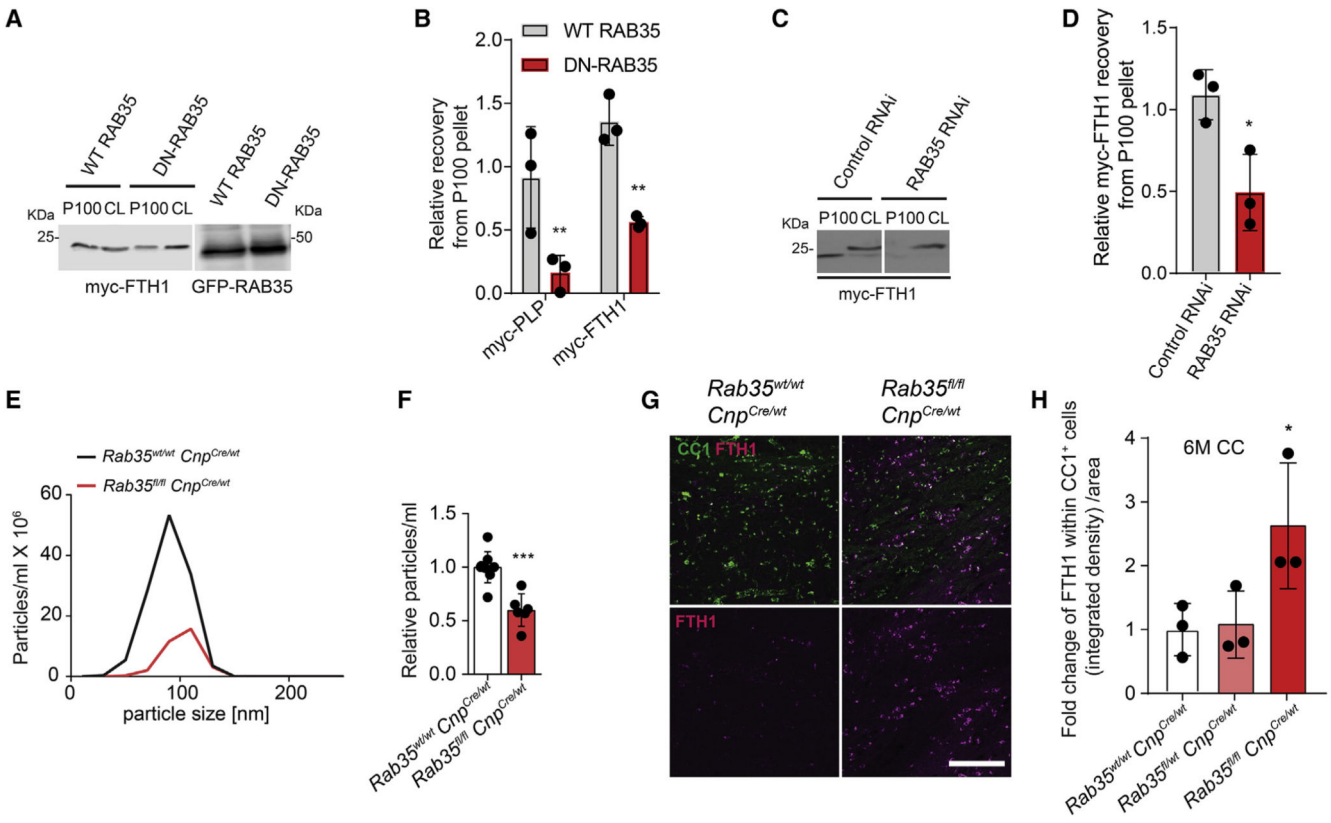

Figure 6. Oligodendrocytes Secrete Ferritin Heavy Chain in a RAB35-Dependent Manner

(A) Western blot of cell lysate (CL) and 100,000*g* pellets (P100) from Oli-neu cells transfected with myc-tagged FTH1 together with wild-type EGFP-RAB35 (WT-RAB35) or dominant-negative EGFP-RAB35^{N120I} (DN-RAB35).

(B) Quantification of relative amounts of myc-FTH1 and myc-PLP in P100 normalized to cell lysates. Data are means ± SD; **p < 0.01 by two-way ANOVA with Sidak's multiple comparison test.

(C) Western blot of cell lysate (CL) and 100,000*g* pellets (P100) from Oli-neu cells treated with control RNAi or RAB35 RNAi and transfected with myc-tagged FTH1.

(D) Quantification of relative amounts of myc-FTH1 in P100 normalized to cell lysates upon knockdown of RAB35. Data are means ± SD; *p < 0.05 by two-tailed Student's t test.

(E) Representative nanoparticle tracking analysis size distribution profile for 100,000*g* pellets obtained from culture medium of *Rab35* KO (Rab35$^{fl/fl}$;Cnp$^{Cre/wt}$) (red) and control oligodendrocytes (Rab35$^{wt/wt}$;Cnp$^{Cre/wt}$) (black).

(F) Quantification of number of particles released in the medium of cultured *Rab35* KO (red) and control (white) oligodendrocytes. Data are means ± SD; ***p < 0.001 by two-tailed Student's t test.

(G) Images of corpus callosum of 6-month-old control (Rab35$^{wt/wt}$;Cnp$^{Cre/wt}$) and *Rab35* KO (Rab35$^{fl/fl}$;Cnp$^{Cre/wt}$) mice immunostained with antibodies against FTH1 and CC1. Scale bar, 100 μm.

(H) Quantification of integrated density of FTH1 immunostaining within $CC1^+$ cell/area. Data are means ± SD; ns, non-significant; *$p < 0.05$ by one-way ANOVA with Dunnett's multiple comparison test.

Europe PMC Funders Author Manuscripts

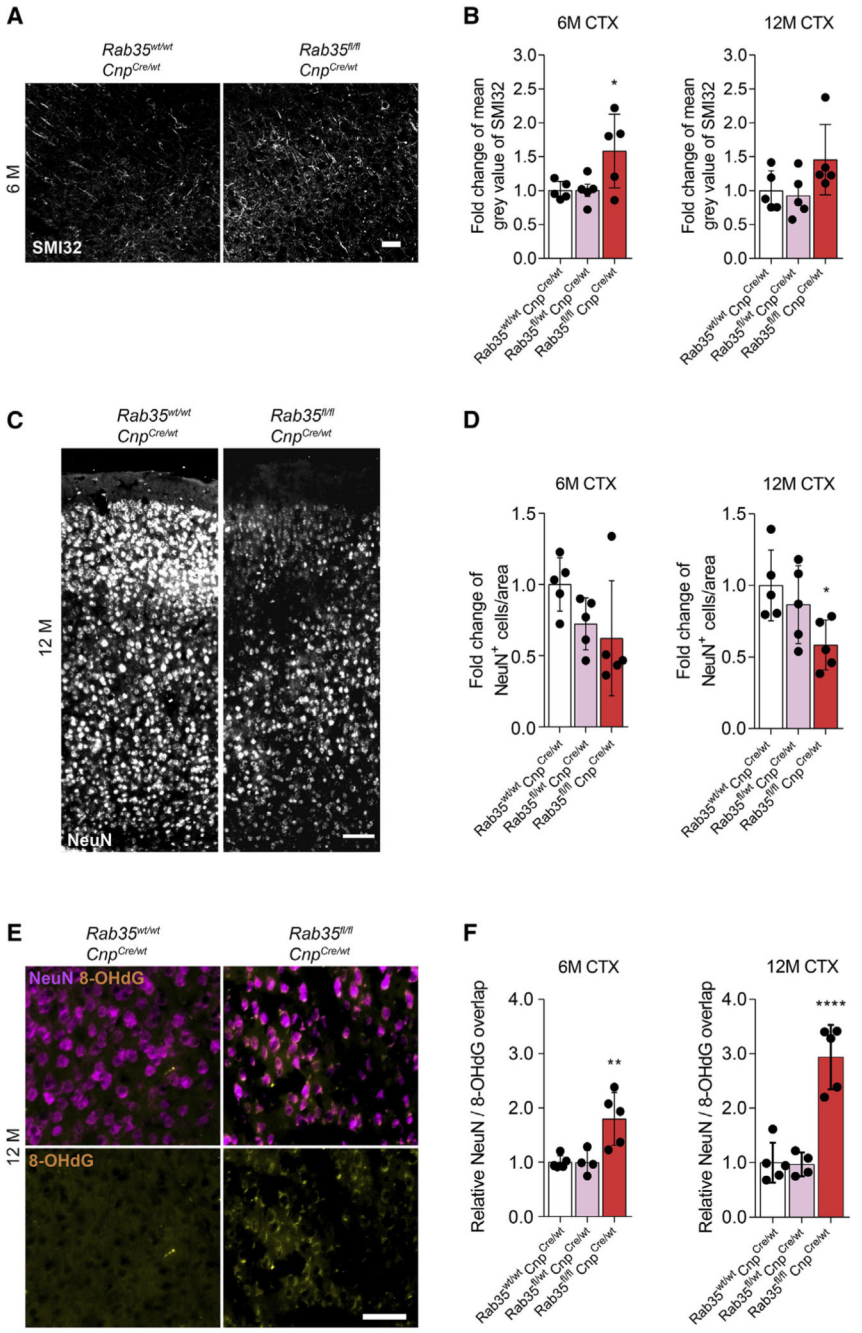

Figure 7. Oligodendrocyte-Specific *Rab35* Knockout Results in Neuronal Loss and Oxidative Damage in Mice

(A) Images of *Rab35* KO and control mice cortex immunostained with antibodies against unphosphorylated neurofilament (SMI32). Scale bar, 100 μm.

(B) Quantification of relative change of mean gray value of SMI32 signal of $Rab35^{wt/wt}$; $Cnp^{Cre/wt}$ (white), $Rab35^{fl/wt}$, $Cnp^{Cre/wt}$ (pink), and $Rab35^{fl/fl}$;$Cnp^{Cre/wt}$ (*Rab35* KO) mice (red) at 6 and 12 months.

(C) Images of *Rab35* KO and control mice cortex immunostained with antibodies against neuronal nuclei (NeuN). Scale bar, 100 μm.

Europe PMC Funders Author Manuscripts

(D) Quantification of relative density of $NeuN^+$ cells/area of 6- and 12-month-old *Rab35* KO and control mice motor cortex.
(E) Images of *Rab35* KO and control mice motor cortex immunostained with antibodies recognizing oxidative DNA modifications (8-OHdG, yellow), and NeuN (magenta). Scale bar, 50 μm.
(F) Quantification of relative overlap of 8-OHdG and NeuN signals of 6- and 12-month-old *Rab35* KO and control mice motor cortex.
In (B), (D), and (F), all data are means ± SD; *p < 0.05, **p < 0.01, ****p < 0.0001 by one-way ANOVA with Tukey's multiple comparison test.
See also Figures S5–S7.

Europe PMC Funders Author Manuscripts